WPJET1-PR(18) 21007

V S Neverov et al.

Determination of isotope ratio in the divertor of JET-ILW by high-resolution H? spectroscopy: H-D experiment and implications for D-T experiment

Preprint of Paper to be submitted for publication in
Nuclear Fusion

This work has been carried out within the framework of the EUROfusion Consortium and has received funding from the Euratom research and training programme 2014-2018 under grant agreement No 633053. The views and opinions expressed herein do not necessarily reflect those of the European Commission.

Determination of isotope ratio in the divertor of JET-ILW by high-resolution H_α spectroscopy: H-D experiment and implications for D-T experiment

V S Neverov[1], A B Kukushkin[1,2,3], U Kruezi[4], M F Stamp[4], H Weisen[4] and JET Contributors[a]

EUROfusion Consortium, JET, Culham Science Centre, Abingdon, OX14 3DB, UK
[1]National Research Centre "Kurchatov Institute", Moscow, 123182, Russia
[2]National Research Nuclear University MEPhI, Moscow, 115409, Russia
[3]Moscow Institute Physics and Technology, Dolgoprudny, Moscow Region, 141700, Russia
[4]CCFE, Culham Science Centre, Abingdon, Oxon, OX14 3DB, UK
[a]See the author list of X Litaudon et al. 2017 *Nucl. Fusion* **57** 102001

E-mail: neverov_vs@nrcki.ru

Abstract. The data of the Hα high-resolution spectroscopy, collected on the multiple lines of sight, which cover the entire divertor space in poloidal cross-section, during the recent hydrogen-deuterium experiments in JET-ILW (ITER-like wall), are processed. A strong spatial inhomogeneity of the hydrogen concentration, H/(H+D), in divertor is found in many pulses. Namely, the H/(H+D) ratio may be lower in the inner divertor than that in the outer divertor by the values of 0.15 – 0.35, depending on the conditions of gas puffing and plasma heating. This effect suggests the necessity of spatially-resolved measurements of isotope ratio in the divertor in the upcoming deuterium-tritium experiments. Also, separation of the overlapped Tα and Dα spectral lines is shown to be a challenging task especially when the local Doppler-broadened (Gaussian) line shapes are noticeably distorted by the net inward flux of fast non-Maxwellian neutral atoms. We use the respective, formerly developed model of an asymmetric spectral line shape, while analysing the data of the first deuterium-tritium experiment in JET-C (carbon wall), and test the model via comparing the isotope ratio results with another diagnostic's measurements. This model is shown to increase the accuracy of tritium concentration measurements in the divertor.

Keywords: tokamak diagnostics, spectral line shapes, inverse problems, isotope ratio

PACS: 52.70.Kz, 52.25.Ya, 32.70.Jz, 02.30.Zz

1. Introduction

In support of deuterium-tritium (D-T) experiments scheduled for 2019-2020, JET conducted the experimental campaign C37 "Hydrogen" with hydrogen-deuterium (H-D) plasmas in 2016 [1]. The campaign was aimed at solving the following tasks:(i) controlling the isotope ratio using various scenarios of fuelling with gas puffing and pellets [2], (ii) investigation of the influence of the isotope ratio on the plasma confinement, L-H transition [3] and density limit in the H-mode [4], (iii) testing

various scenarios of plasma heating using neutral beam injection (NBI) and/or ion-cyclotron resonance (ICRH) [5, 6], etc. [1]. The hydrogen concentration was varied from 1% to 99% during the campaign.

In JET, the main instrument for measuring the isotope ratio in the scrape-off layer (SOL) and the divertor is the passive Hα high-resolution spectroscopy (HRS). The HRS measurements in the main chamber SOL are complicated by the problem of signal decomposition, namely, separation of the light from high-field side (HFS) SOL, low-field side (LFS) SOL and, in many pulses, the divertor stray light (DSL), i.e. the light emitted in the divertor and reflected by beryllium walls to the detector [7]. Also, due to the low plasma density in the SOL one must deal with the strong asymmetry of the line shapes, caused by the net inward flux of fast non-Maxwellian neutral atoms. All of this reduce the accuracy of isotope ratio measurements in the main chamber SOL. This paper is dedicated to the measurements in the divertor only.

Our interest in the Hα HRS measurements in divertor originated from the problem of determining the influence of DSL on the Hα measurements in the main chamber [7], a major problem for the Hα diagnostics in ITER [8, 9]. The predictive modelling of the DSL spectrum in JET in [7] required the recovering of the parameters of neutral atoms in the divertor, including the isotope ratio. A high spatial resolution was necessary. At JET, the latter was achieved due to the 16 lines of sight (LoSs) covering the entire divertor space in poloidal cross-section. The standard software for interpreting the HRS spectra, which operates in JET for more than 20 years, processes the data from the two LoSs only, namely, one LoS per inner and outer divertor. So, a new software was created [7] to process the data from all the LoSs. This new software sequentially solves the following tasks for a given pulse: (i) recovering the spatial distribution of the isotope ratio and temperature of the neutral hydrogen in the divertor, (ii) predictive modelling of the DSL spectral line shape on the LoS in the main chamber, (iii) decomposing the signal on the LoS in the main chamber, namely, separating the light from the high-field side (HFS) SOL, low-field side (LFS) SOL and the DSL, as well as recovering the isotope ratio and temperature of the neutral hydrogen in the main chamber SOL. The accuracy of solving the task ‘iii’ is obviously lower than that of the task ‘i’.

When processing the data of the C37 experimental campaign with the software [7], a strong difference in hydrogen concentration, H/(H+D), measured on different LoSs was observed in many pulses. The H/(H+D) ratio was always lower in the inner region of the divertor. The spatial inhomogeneity of the isotope ratio is increased when gas introduction modules (GIMs) located in the divertor are used or when certain scenarios of NBI and ICRH heating were applied. In different pulses under similar conditions a similar spatial distribution of hydrogen isotopes was observed. This paper does not carry a quantitative analysis of this effect, which would require a complex numerical simulation, but merely attempts to systematize the observations and give a qualitative explanation.

Based on the results for H-D plasma, one can expect spatial inhomogeneity of the isotope ratio in the divertor in the upcoming deuterium-tritium (D-T) experiment. Therefore, spatially resolved measurements are relevant for D-T plasma as well. However, the tritium when present in the mixture significantly complicates the interpretation of the measured spectrum since the Dα and Tα lines, being three times closer than Hα and Dα lines, almost merge into one due to the Doppler broadening. To obtain accurately the tritium concentration, T/(H+D+T), the model of the Balmer-alpha line shape, used for H-D plasma, requires a modification. Even a weak asymmetry of the Dα line shape caused by the influx of neutral atoms from the wall into the plasma leads to an overestimation of tritium concentration if this asymmetry is not featured in the model. The line shape model proposed in [10, 11] takes the asymmetry into account. The only way to test it on a real deuterium-tritium experiment is to apply it to the data of the DTE1 experiment, the first such experiment conducted in JET-C (carbon wall) in 1997. This test is done in this paper.

The paper is organized as follows. Sec. 2 describes determination of the isotope ratio in H-D plasma in the divertor of JET-ILW during the C37 campaign. First, the results of the software [7] which processes the data from 16 LoSs are compared with the results of the standard software on JET for processing the Hα HRS measurements. Further, the time- and spatially-resolved values of H/(H+D) ratio in the divertor are given for several characteristic pulses differing by the parameters of gas puffing and plasma heating. Sec. 3 deals with determination of the isotope ratio in D-T plasma. First, the advantages of the

asymmetric line shape model are demonstrated. Then, this model is tested against the data of DTE1 experiment in JET-C. Conclusions are given in Sec. 4.

2. Determination of isotope ratio in H-D plasma

The layout of the LoSs in the divertor of JET-ILW is shown in figure 1. This figure also features the location of Langmuir probes the data from which are shown below in multiple figures. We used 16 LoSs located in the 1st octant and viewing from the vessel's top down at divertor. These LoSs cover the entire divertor space in poloidal cross-section. The LoSs observing the inner divertor are marked with the letter "i", while those observing the outer divertor are marked with "o". The signals are collected by a pair of fibre-fed HRS systems: KSRD and KSRB with spectral resolution = 0.0052 nm/pixel and instrumental FWHM = 0.024 nm. The resulting spectra contain only central π-component as the Zeeman σ-components are filtered out.

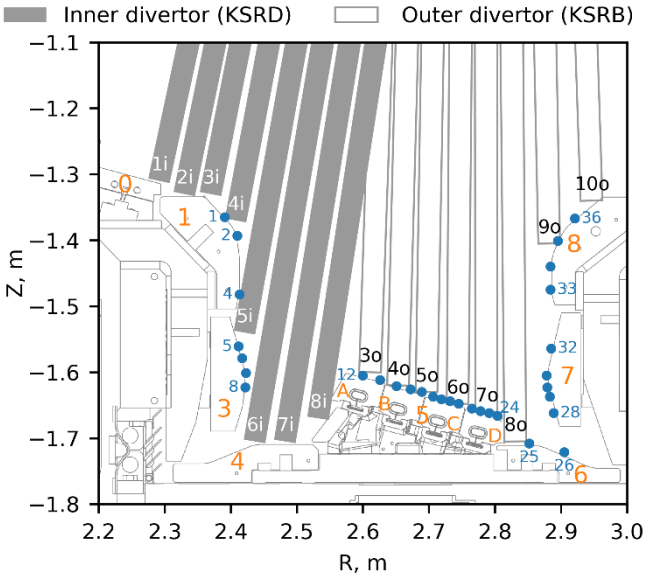

Figure 1. The layout of LoSs 1i – 8i (grey bars) of the inner divertor and LoSs 3o– 10o (white bars) of the outer divertor viewing from the vessel's top down at divertor of JET-ILW. The bars show projections of observation cones on the poloidal plane. The circles show the location of working Langmuir probes. The large digits denote the tile numbers. The letters A, B, C, D denote the stacks of tile 5.

The inverse problem of fitting the experimental spectrum with the theoretical one is formulated in [12]. For the theoretical spectrum the equation (1) from [7] is used, which is given below:

$$S^{\text{theor}}(\lambda_j) = \sum_{t=1}^{M} x_t \sum_{i=\text{H,D,T}} X_i F_{\text{Gauss}}\left(\lambda_j - \lambda_i^{\text{alpha}}, T_t, m_i\right), \quad (1)$$

$$F_{\text{Gauss}}\left(\lambda - \lambda_i^{\text{alpha}}, T_t\right) \equiv \frac{1}{\lambda_i^{\text{alpha}}}\sqrt{\frac{m_i}{2\pi T_t}}\, exp\left(-\frac{m_i}{2T_t}\left(\frac{\lambda - \lambda_i^{\text{alpha}}}{\lambda_i^{\text{alpha}}}\right)^2\right). \quad (2)$$

Here j is the index of the pixel (spectral channel), i is the hydrogen isotope index, m_i is the mass of the i-th hydrogen isotope, λ_i^{alpha} is the wavelength of the Balmer-alpha line centre for the i-th isotope, t is the index of the fraction of atoms with the temperature T_t, M is the total number of the temperature values that characterize the spatial profile of the emissive layer along the LoS. The sought-for parameters are: T_t is the temperature of the atoms of the fraction t, x_t is the partial contribution (statistical weight) of the t–th fraction of atoms to the total intensity, X_i is the partial contribution of the i-th isotope to the integral intensity, which is assumed to be equal to the concentration of this isotope in the mixture.

The inverse problem is solved for $M = 3$ and i = H, D for each LoS independently using the sequential least squares programming method. The bounds and the default initial guesses for the sought-for parameters are given in the table 1 in [7]. Using the condition $X_D = 1 - X_H$, the problem has 7 sought-for parameters.

Note that the Stark effect is not considered here. The reason for that is the poor sensitivity of Balmer-alpha line shape to the Stark broadening, especially when the electron density is less than 10^{20} m^{-3} [13]. As far as the model line shape without Stark effect fits the experimental data well, the account of the Stark broadening in the model with the electron density as an additional sought-for parameter will complicate the ill-conditioned inverse problem even more that would negatively impact the accuracy.

It is worth to compare the new results with those obtained with the standard software for processing the Hα HRS data in JET. This standard software uses only two LoSs: one LoS per inner and outer divertor. Among all the LoSs a LoS with the most narrow and symmetric Balmer-alpha line shape is selected. A sufficient signal strength with no saturation on a flat-top stage of a given pulse is also an important factor. In the latest experimental campaigns, the LoS 7i and LoS 9o met these criteria. The theoretical spectrum used in this software is slightly different from (1):

$$S_{\mathrm{cw}}^{\mathrm{theor}}(\lambda_j) = \sum_{i=\mathrm{H,D,T}} \left(x_{c,i} F_{\mathrm{Gauss}}\left(\lambda_j - \lambda_i^{\mathrm{alpha}} - \Delta\lambda_{\mathrm{c}}, T_c\right) + x_{w,i} F_{\mathrm{Gauss}}\left(\lambda_j - \lambda_i^{\mathrm{alpha}} - \Delta\lambda_w, T_w\right)\right). \quad (3)$$

Here the sought-for parameters are: T_c and T_w are the temperatures of the cold and warm fractions of atoms, respectively, whose values are the same for all isotopes; $x_{c,i}$ and $x_{w,i}$ are the partial contributions (statistical weights) of the cold and warm fraction of atoms, respectively, of the i-th isotope to the total intensity; $\Delta\lambda_{\mathrm{c}}$ and $\Delta\lambda_{\mathrm{w}}$ are the wavelength shifts of the maxima of the Gaussian functions relative to the line centre $\lambda_i^{\mathrm{alpha}}$ for the cold and warm fractions of atoms. respectively.

Like in the model spectrum S^{theor} (1), in the $S_{\mathrm{cw}}^{\mathrm{theor}}$ (3) the sought-for parameters are optimized, being variable within certain bounds. For example, the values of $\Delta\lambda_c$ and $\Delta\lambda_w$ mast be smaller than $\left|\lambda_D^{\mathrm{alpha}} - \lambda_T^{\mathrm{alpha}}\right|$. For a two-isotope mixture, the number of unknowns is 8 and for a three-isotope mixture it's 10.

Unlike the S^{theor} spectrum (1), the $S_{\mathrm{cw}}^{\mathrm{theor}}$ (3) lacks the hot fraction of atoms which is crucial for good fitting of the far wings of the line shape. At the same time, the spectrum $S_{\mathrm{cw}}^{\mathrm{theor}}$ has some advantages: different isotopes can have different partial contribution of each fraction of atoms (cold or warm), the wavelength shifts $\Delta\lambda_{\mathrm{c}}$ and $\Delta\lambda_{\mathrm{w}}$ allow the model to address a weak line shape asymmetry, although the asymmetry can be modelled more accurately (see [10] and equations (6)-(8) below). Note that we did not perform any calculations with the $S_{\mathrm{cw}}^{\mathrm{theor}}$ spectrum for this work. All the results obtained with this spectrum that are shown below were taken from the JET database.

The $S_{\mathrm{cw}}^{\mathrm{theor}}$ spectrum allows to obtain the isotope concentration either by using the cold fraction of atoms only or the both fractions. These concentrations are denoted as $X_{c,i}$ and $X_{cw,i}$ respectively:

$$X_{c,i} = \frac{x_{c,i}}{\sum_{j=\mathrm{H,D,T}} x_{c,j}}, X_{cw,i} = \frac{x_{c,i} + x_{w,i}}{\sum_{j=\mathrm{H,D,T}}\left(x_{c,j} + x_{w,j}\right)} \quad (4)$$

Note that the software returns the value of $X_{c,i}$ as the isotope concentration by default.

Figure 2 shows the best fit of the spectra on LoS 7i and LoS 9o with the theoretical line shapes S^{theor} and $S_{\mathrm{cw}}^{\mathrm{theor}}$ at time t = 20.1 s of the pulse 90999. One can see that the S^{theor} fits both spectra slightly better than the $S_{\mathrm{cw}}^{\mathrm{theor}}$. Also notice the difference of 0.021 between the X_H (S^{theor} spectrum) and $X_{c,H}$ ($S_{\mathrm{cw}}^{\mathrm{theor}}$ spectrum) on LoS 7i as well as the difference of 0.01 between the $X_{c,H}$ and $X_{cw,H}$.

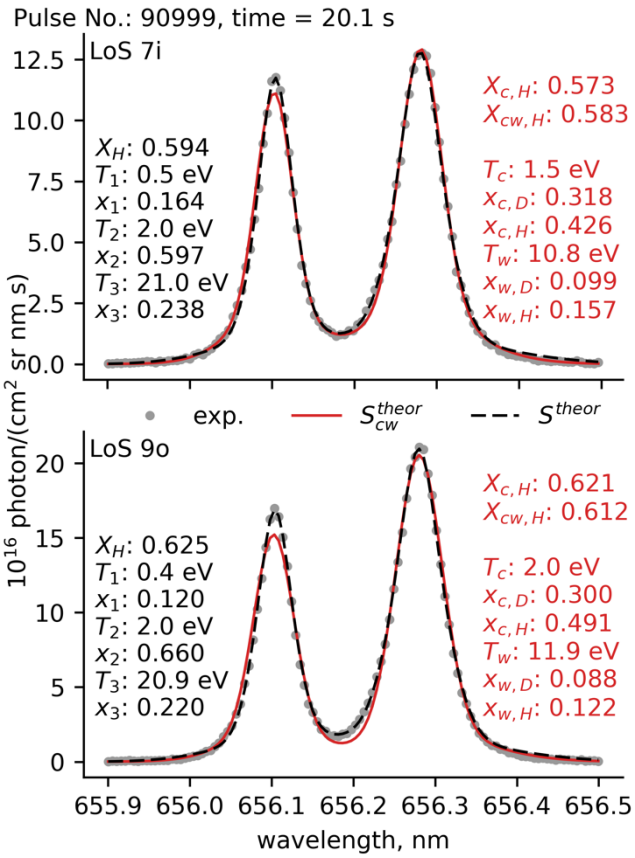

Figure 2. Best fit of the experimental spectra on LoS 7i (top) and LoS 9o (bottom) with the theoretical spectra S^{theor} (1) and $S_{\text{cw}}^{\text{theor}}$ (3) at time t = 20.1 s of the pulse 90999. The optimal parameters of the S^{theor} and $S_{\text{cw}}^{\text{theor}}$ are shown in the left and right columns respectively.

To test the model spectra S^{theor} and $S_{\text{cw}}^{\text{theor}}$ on a large set of data, we calculate the time-average absolute differences of hydrogen concentration obtained with these model spectra:

$$\Delta X_{c,H} = \frac{1}{N}\sum_{k=1}^{N}\left|(X_H)_k - \left(X_{c,H}\right)_k\right|, \Delta X_{cw,H} = \frac{1}{N}\sum_{k=1}^{N}\left|(X_H)_k - \left(X_{cw,H}\right)_k\right|, \quad (5)$$

where k is the index of a single measurement made at certain time moment of the pulse and N is the total number of such measurements during the pulse. Similarly, one can define the value of $\Delta X_{c\text{-}cw,H}$ for the difference between the $X_{c,H}$ and $X_{cw,H}$, which characterizes the uncertainty of the hydrogen concentration found using the spectrum $S_{\text{cw}}^{\text{theor}}$.

Figure 3 shows the values of $\Delta X_{c,H}$, $\Delta X_{cw,H}$ and $\Delta X_{c\text{-}cw,H}$ for a set of 80 pulses of the C37 campaign, juxtaposed to the time-average hydrogen concentrations found using the spectrum S^{theor} for the LoS 7i and LoS 9o.

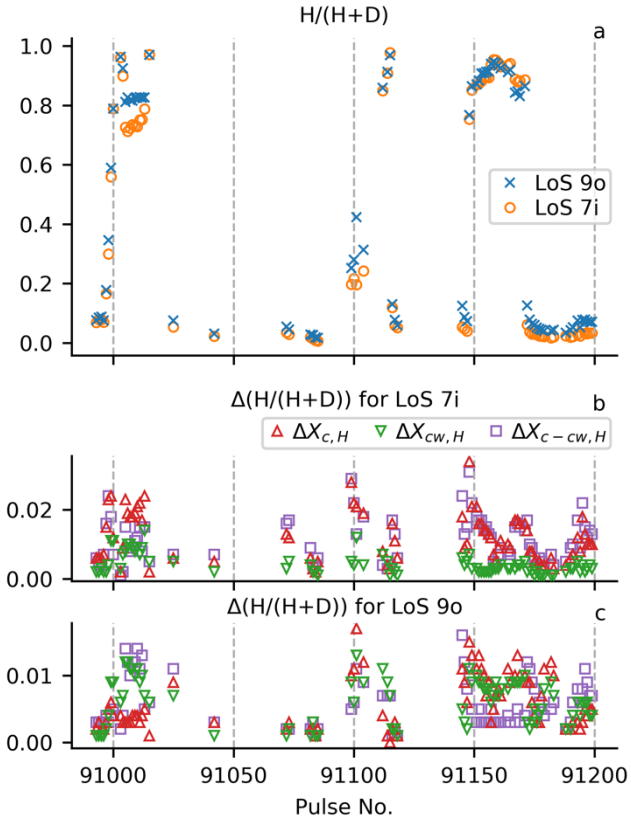

Figure 3. (a) The time-average hydrogen concentrations on the LoS 7i and LoS 9o as a function of pulse number; (b) the time-average absolute differences of hydrogen concentrations $\Delta X_{c,H}$, $\Delta X_{cw,H}$ and $\Delta X_{c\text{-}cw,H}$ (see equation (5)) for the LoS 7i as a function of the pulse number; (c) the same as 'b' but for the LoS 9o.

One can see that the values of $\Delta X_{c,H}$, $\Delta X_{cw,H}$ and $\Delta X_{c\text{-}cw,H}$ do not depend on hydrogen concentration. For the LoS 9o all three values are about 0.01 that is the typical error for determining the hydrogen concentration using the HRS. For the LoS 7i the values of $\Delta X_{c,H}$ and $\Delta X_{c\text{-}cw,H}$ are about 0.02, but not the values of $\Delta X_{cw,H}$ which are about 0.01. This means that for the LoS 7i the hydrogen concentration found using the S^{theor} spectrum is in good agreement with that found using the $S_{\text{cw}}^{\text{theor}}$ spectrum only if the both (cold and warm) fractions of atoms are used to calculate the concentration. Anyway, the uncertainty of the $S_{\text{cw}}^{\text{theor}}$ spectrum itself characterized by the values of $\Delta X_{c\text{-}cw,H}$ is as high as the discrepancy between the results obtained with the two different model spectra. So, in determining the isotope ratio in H-D plasma the software [7] which uses the S^{theor} spectrum is at least as accurate as the old software which uses the $S_{\text{cw}}^{\text{theor}}$ spectrum. In section 3 it will be shown that this is not true in the case of D-T plasma.

In figure 3, one can notice the significant difference between the time-average hydrogen concentration on LoS 7i and 9o in some pulses. The inhomogeneity of the isotope ratio in the divertor is analysed below in detail. This inhomogeneity depends on plasma configuration. It increases when certain GIMs are used for gas puffing or when the plasma heating is on, so let us show first the layout of the gas introduction and plasma heating systems in JET. Figure 4 shows the layout of ten GIMs, the GIMs 9 - 12 are located directly in the divertor. Note that the GIMs 11 and 12 are located in the inner part of divertor while the GIMs 9 and 10 are located in the outer part. The divertor GIMs have multiple gas valves evenly distributed along the toroidal direction. Figure 5 shows the layout of two NBI modules, ICRH antennas including the ITER-like antenna (ILA) and the pellet injector.

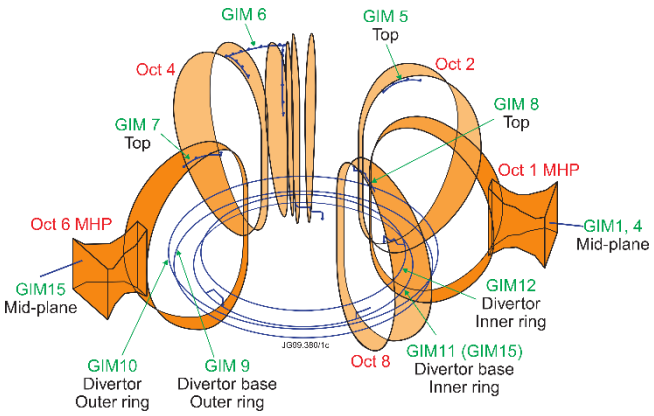

Figure 4. The layout of gas introduction modules (GIMs) in JET. The GIMs 9 - 12 have multiple gas valves evenly distributed along the toroidal direction.

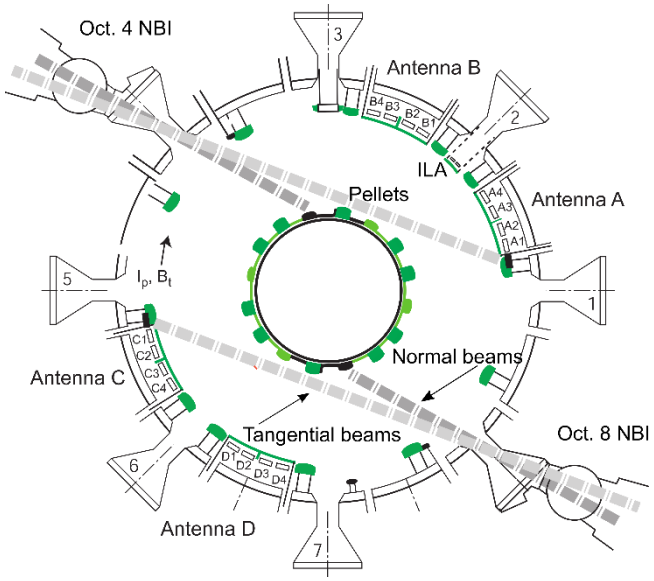

Figure 5. The layout of JET plasma heating systems (courtesy: Ph. Jacquet, CCFE, UK): the neutral beam injectors (NBI), ion-cyclotron resonance antennas including the ITER-like antenna (ILA) and pellet injector.

We noticed that in all processed pulses the values of H/(H+D) ratio are very close on some neighbouring LoSs, namely the pairs 1i and 2i, 7i and 8i and the group 7o, 8o, 9o. Therefore, for these neighbouring LoSs, the group-average H/(H+D) ratios are shown in the figures 6 – 11 below.

Figure 6 shows the time-average spatially-resolved hydrogen concentration in the divertor for most of the pulses in mixed H-D plasma of the C37 campaign. The limiter pulses and the pulses in H(D)-only plasma are not shown. The usage of NBI, ICRH and pellets is shown with the background colour. The four small dots under the *x*-axis show the gas type (D_2, H_2 or none) injected via the divertor GIMs 9 – 12 in the given pulse.

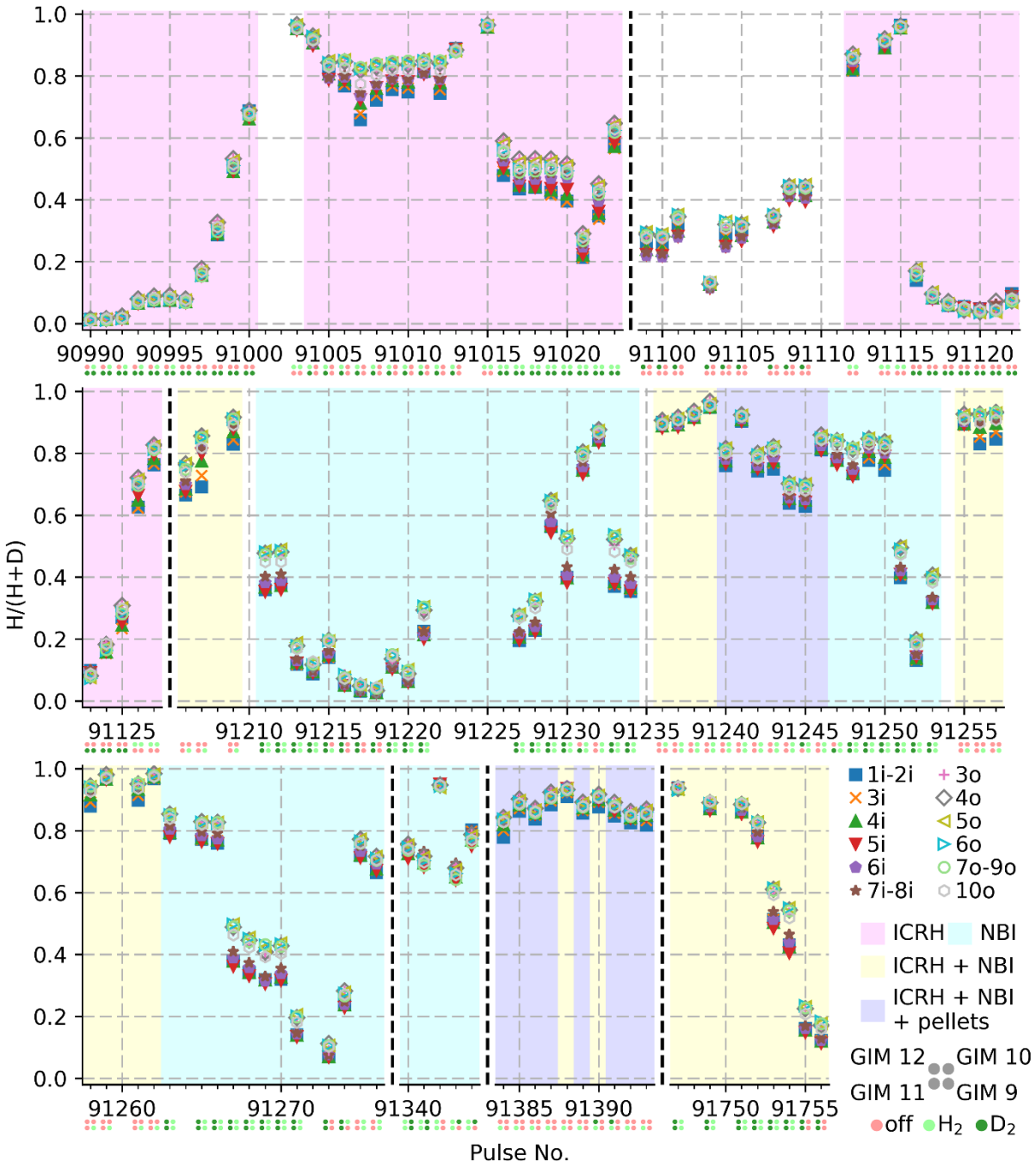

Figure 6. The time-average spatially-resolved hydrogen concentration in the divertor for the pulses in mixed H-D plasma of the C37 campaign. Background colour shows the usage of ICRH, NBI and pellets. The four small dots under the *x*-axis show the gas type (D_2, H_2 or none) injected via the divertor GIMs 9 – 12 in the given pulse (see the legend).

Figure 6 shows the following regularities: (i) the time-average H/(H+D) ratio in the inner divertor is usually lower than that in the outer divertor; (ii) in many pulses with ICRH, the lowest time-average H/(H+D) ratio is observed on the LoSs 1i-2i; (iii) in many pulses without ICRH, the LoSs 1i-6i give very close values of the time-average H/(H+D) ratio, while the lowest value is usually observed on the LoS 5i; (iv) if the ICRH is not used, the significant difference in the time-average H/(H+D) ratio between the inner and outer divertor is observed only if the inner divertor GIMs 11 and 12 are used for D_2 puffing and the outer divertor GIMs 9 and 10 are used for H_2 puffing; (v) in the most pulses where the GIM 11 is used, it is used for D_2 puffing.

In the pulses 91341, 91343 and 91344, the time-average H/(H+D) ratio in the inner divertor is slightly higher than that in the outer divertor. Unlike it is in many other pulses, here the H_2 (and not D_2) is injected via the inner divertor GIM 11. However, the usage of the inner and outer divertor GIMs for injection of different gasses cannot of itself explain the spatial inhomogeneity of the isotope ratio in divertor in the cases where these GIMs were not used or were used at low power. The recycling of hydrogen isotopes at the divertor tungsten-coated tiles also plays a significant role. It is very likely that some of the deuterium injected via the GIMs 11 and 12 is absorbed by the tiles 0, 1 and 3. This trapped deuterium is released during the subsequent pulses in the cases where the heat loads on divertor tiles are high enough, e.g. due to the use of ICRH. The recycling of hydrogen isotopes and its impact on plasma fuelling is under active study [14, 15]. It was shown that the inner divertor (especially the tile 1) is characterized by higher level of recycling compared to the outer divertor [15].The post mortem analysis of JET-ILW divertor tiles after 2010 – 2012 [16] and 2013 – 2014 campaigns [17] shows that the concentration of deuterium retained in the tiles has its maximum on the top of tile 1, decreasing with increasing tile's number (see figure 3 in [16] and figure 5 in [17]). The total amount of D atoms retained in the divertor after 2010 – 2012 experimental campaign was $2.4 \cdot 10^{23}$ while 83% of atoms deposited in the inner divertor and 54% of atoms in the tiles 0 and 1 only [16]. The study of D_2 and H_2 desorption [18] shows not only higher desorption rates for the inner divertor tiles than for the outer ones but also higher desorption rates of D_2 compared to those of H_2 and HD at the temperatures between 350° and 550° C (see figure 5 therein). The latter fact can lead to an excess of deuterium concentration in the inner divertor even in those cases where the amounts of deuterium and hydrogen in the tiles are equal.

The maximum difference in the time-average H/(H+D) ratio (~0.2) between the LoSs 1i-2i and the LoSs of the outer divertor is observed in the pulses 91007 and 91207. At certain time moments during the pulses the difference in H/(H+D) ratio can be as high as 0.35. To understand how the measured isotope ratio is correlated with other parameters, e.g. the measured photon fluxes, gas injection rates, ICRH and NBI powers, one has to analyse these parameters as a function of time.

Figures 7 – 11 below show the time evolution of spatially-resolved hydrogen concentration in the divertor, juxtaposed with other major parameters of the discharge for 5 characteristic pulses of the C37 campaign. Similar plots for many other pulses of this campaign are available online as a supplementary material. The H/(H+D) ratios are not shown when the signal on the LoS is saturated, or too weak (< 1000 counts for all pixels). The curves of the Balmer-alpha photon flux for the grouped LoSs 1i-2i, 7i-8i and 7o-9o show the maximum value among the LoSs in the group. For a more complete characterization of recycling of hydrogen isotopes, the ion fluxes measured by the Langmuir probes are shown for those parts of divertor tiles which the LoSs are looking at or passing close to. The location of Langmuir probes is shown in figure 1. We grouped the probes into sets according to their closeness to certain LoSs. One can see that the LoSs 1i, 2i and 3i do not observe any probes, the LoS 4i observes the probes 1 and 2, the LoS 5i observes the probes 5 and 6 and passes close to the probe 4, the LoS 6i passes close to the probes 7 and 8, etc. Here is the complete list of these groups and the corresponding LoSs.

LoSs	Probes
4i	1, 2
5i	4 – 6
6i	7 – 8
3o	12, 13
4o	14, 15
5o	16 – 18
6o	19 – 21
7o – 9o	22 – 35
10o	36

For each group, the maximum value of ion flux among all the probes in the group is shown. Unfortunately, we have no data for the ion flux on the tile 0 and the top part of tile 1, which we expect can be higher than that near the strike points when the ICRH is used.

In JET the isotope ratio is also measured in subdivertor region using the Penning gauge coupled with another HRS system. The Penning gauge is installed in the vacuum pipe connected to one of the lower

divertor ports located in the outer divertor [19]. The plasma temperature in Penning discharge is about 5 eV which yields narrow spectral line shapes. The resulting spectra are processed also using the $S_{\mathrm{cw}}^{\mathrm{theor}}$ spectrum. This diagnostic is essential for measuring the tritium concentration in D-T plasma, but it is also interesting to compare its results with the measurements in the divertor for H-D plasma.

We start from the pulse with the ICR heating of the ^{3}He ions [20, 21] in L-mode. Figure 7 shows the time evolution of the pulse 91007. The gas injection rates as well as the electron density and temperature are shown along with the ion flux, Balmer-alpha photon flux and hydrogen concentration in the divertor. The strike point's locations during the time interval 7.5 s < t < 15 s are the upper part of tile 3, and the stack C of tile 5 while before and after this interval the locations are the lower part of tile 3 and the left part of tile 6, respectively. The gas injection rates are relatively low here, so all the LoSs show very close results for H/(H+D) ratio before the ICRH starts. But when it starts, the photon flux on the LoSs 1i – 3i significantly increases so does the deuterium concentration. Just before the ICRH stops at t = 14 s, the difference of H/(H+D) ratio on the LoSs 1i – 2i and 7o – 9o exceeds 0.3. Since the photon flux on the LoSs 1i – 3i is very high in this pulse, one can expect a high ion flux on the top of tile 1. Unfortunately, no Langmuir probes are installed there. Good correlation between the ICRH power and the photon flux on the LoS 1i – 3i indicates that the high deuterium concentration in the inner divertor is very likely the result of outgassing. Other pulses from the series: 91008 – 91012, show similar behaviour, yet starting with the pulse 91008 more time is required to achieve significant photon flux and high deuterium concentration on the LoSs 1i – 3i. The figures for these pulses can be found in the supplementary material. Note that because these pulses were at the beginning of the C37 campaign, the tiles 0 and 1 might release the deuterium absorbed before this campaign during the long-time operation in D-only plasma.

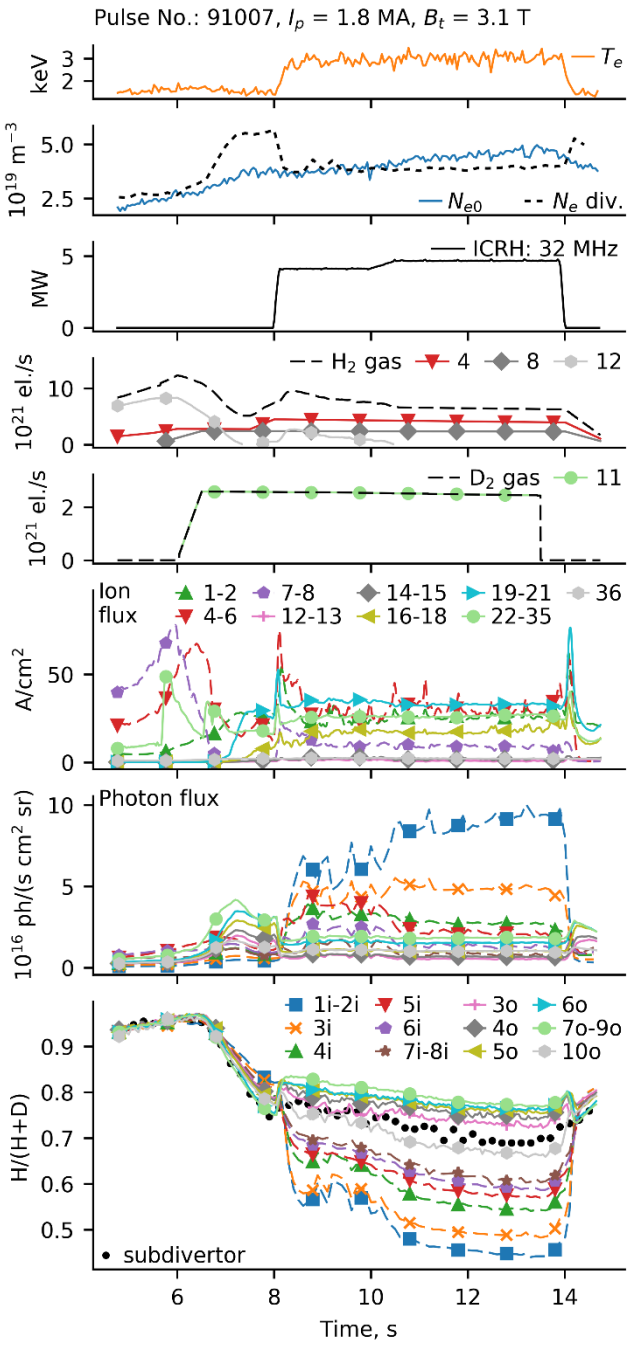

Figure 7. Time evolution of the pulse 91007 (L-mode). From top to bottom: electron temperature on magnetic axis, electron density on magnetic axis (solid curve) and in the divertor measured on the vertical LoS (R = 2.7 m) of the far infrared interferometer (dashed curve), ICRH power (the resonance frequency is indicated in the label), GIM-resolved H_2 and D_2 injection rates in electrons per second (GIM's numbers are shown in the legend), probe-resolved ion flux, LoS-resolved Balmer-alpha photon flux and hydrogen concentration in the divertor. The two bottom plots share the same legend. Black dots on the bottom plot show the H/(H+D) ratio in the subdivertor measured in the Penning gauge. The values of plasma current and magnetic field strength on magnetic axis during the flat-top are given next to the pulse number.

An interesting effect is observed when ICRH is used in the pulses with L-H transition. We demonstrate it on the example of the pulse 91017 shown in figure 8. This effect was also observed in the similar pulses 91016, 91018 and in lesser degree in the pulses 91019, 91022 and 91023, figures for which are available in the supplementary material. In the time interval 7.5 s < t < 25 s the strike point locations are the same as in the pulse 91007. No divertor GIMs are used after 8th second. In this pulse the ICRH power

increases slowly, so does the photon flux on the LoSs 1i – 5i and the deuterium concentration on the same LoSs until the moment of L-H transition at t = 14.3 s when the photon flux on these LoSs drops, so does the deuterium concentration. At the same time the hydrogen concentration in the outer divertor increases, but it also drops at t = 14.3 s. At maximum the difference of H/(H+D) ratio in the inner and outer divertor reaches 0.25. In the H-mode, it remains at the level of 0.15 in this pulse or at the level of 0.2 in the pulses 91022 and 91023.

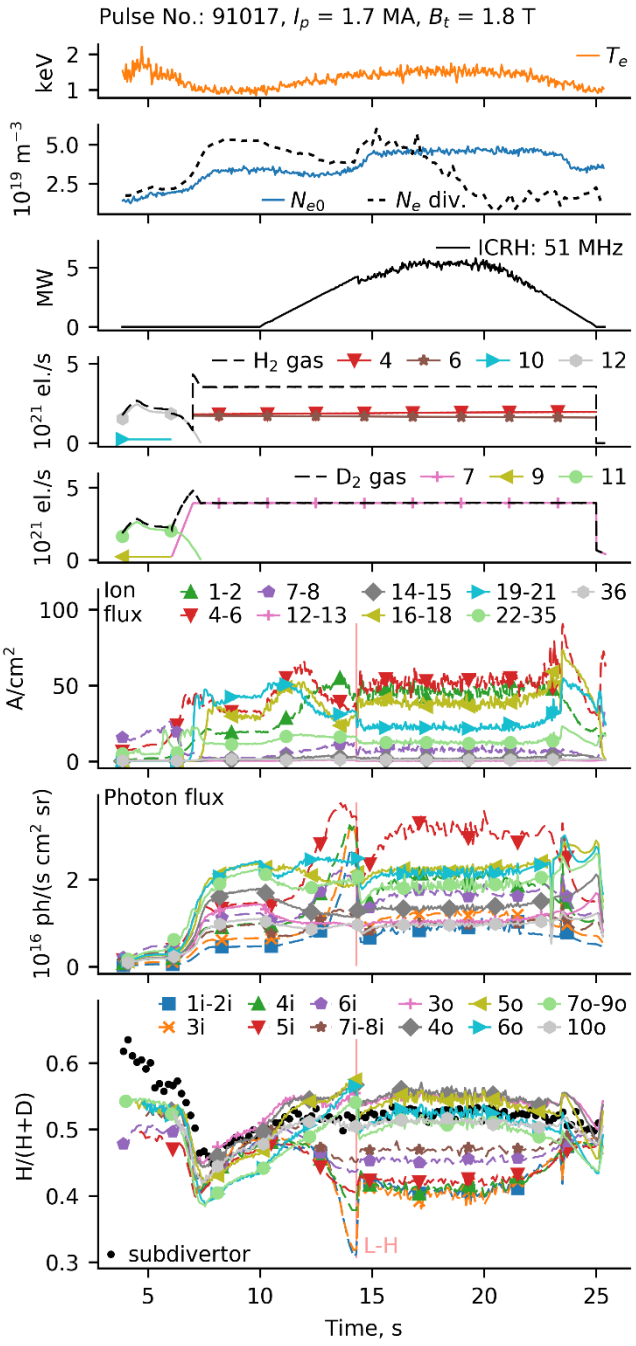

Figure 8. Time evolution of the pulse 91017 (with L-H transition). See the caption of figure 7. The vertical line shows the moment of L-H transition at t = 14.3 s.

Figure 9 shows the time evolution of the ohmic pulse 91100. Here the plasma configuration is different from that in the pulses 91007 and 91017. The strike point's locations during the time interval 4 s < t < 14 s are the lower part of tile 3, and the left part of tile 6 while before and after this interval the locations are the upper part of tile 3 and stack D of tile 6, respectively. The GIMs 7 and 8 located at vessel's top

in the 7th and 8th octant, respectively, are used here for intensive gas puffing. The location of GIMs 7 and 8 excludes the direct impact of the injected gas on the measurements. The divertor GIM 12 is used only in the beginning and in the end of the discharge. The figures for similar pulses: 91099, 91101, 91105, 91107 – 91109 can be found in the supplementary material. In the pulse 91100 the maximum difference in hydrogen concentration of 0.15 is observed between the LoS 6i of and LoS 6o. The signals on the LoS 5i and 6i exhibit the highest photon flux and also the highest deuterium concentration among all the LoSs. Also, the ion fluxes are significantly higher near the inner strike point than near the outer one. Note that in each next pulse in this series (all of them are starting from the low hydrogen concentration) the inhomogeneity of the H/(H+D) ratio is getting smaller and smaller and almost disappears in the pulses 91107 –91109. The difference in the photon flux between the LoS 6i and the LoSs 7o – 9o is also getting significantly smaller.

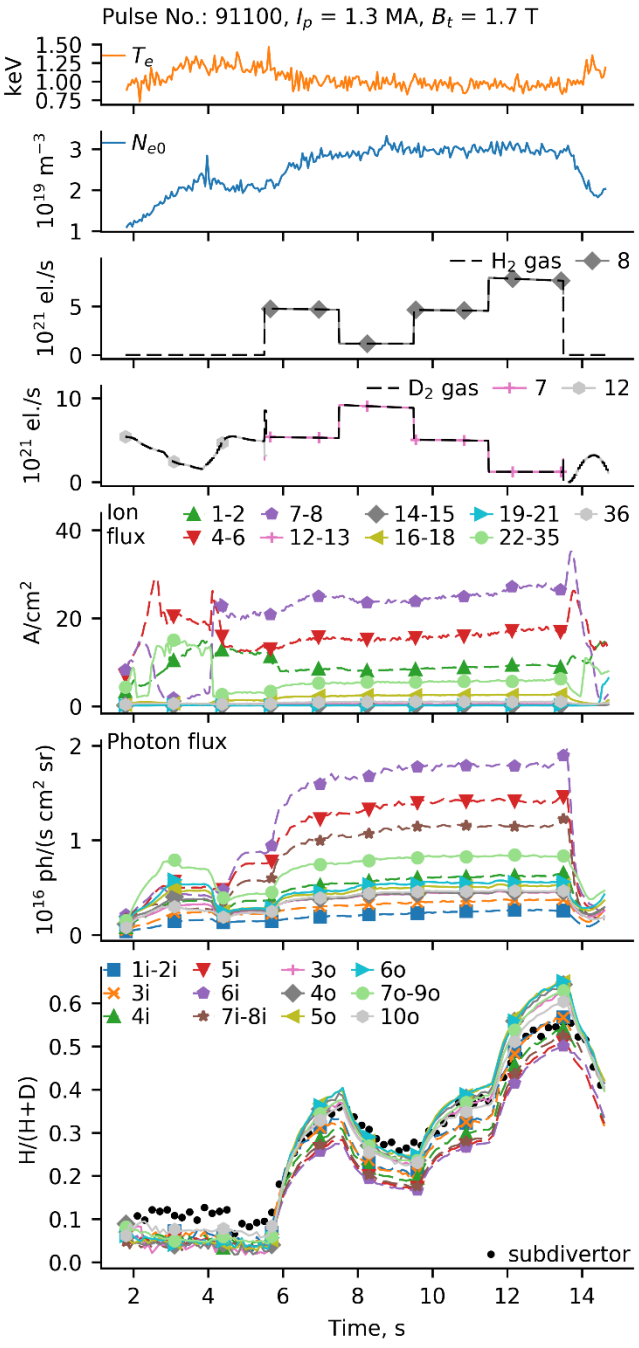

Figure 9. Time evolution of the pulse 91100. See the caption of figure 7.

Next, we show the results for the pulse with ICR heating of D-NBI ions [20, 5] in L-mode. Figure 10 shows the time evolution of the pulse 91209. Here no D_2 is injected via GIMs. The spikes on the curves for the ion and photon fluxes are caused by ELMs. Here the spatial distribution of the hydrogen isotopes in the divertor is similar to that in the pulse 91007. The only difference is that the inhomogeneity of the H/(H+D) ratio is correlated with the NBI and not with the ICRH. At maximum the difference in H/(H+D) ratio between the LoSs 1i – 2i and 3o – 9o reaches 0.2. Like in the pulse 91007, the tiles 0 and 1 release the deuterium absorbed previously but unlike the pulse 91007, this one was performed in the middle of the C37 campaign. So, the excess in deuterium concentration in the tiles 0 and 1 was likely created during this campaign and not during the previous one in D-only plasma. The figures for similar pulses: 91207, 91255 – 91258, 91261, 91262, can be found in the supplementary material. The pulses 91255 and 91262 are of special interest. In the pulse 91255 the deuterium neutral beams are injected in four short (~0.6 s) pulses of the same power (~ 2 MW). The first such NBI pulse occurs before the ICRH is turned on, and no significant drops of the H/(H+D) ratio are detected in the inner divertor, while the three other NBI pulses occur during the ICRH and all three are accompanied with significant drops of the H/(H+D) ratio on the LoSs 1i – 3i. The pulse 91262 is a pulse in hydrogen with H-NBI. Yet when the hydrogen neutral beams are injected the deuterium concentration increases from 0.02 to 0.06 on the LoSs 1i – 3i and from 0.02 to 0.04 on other LoSs.

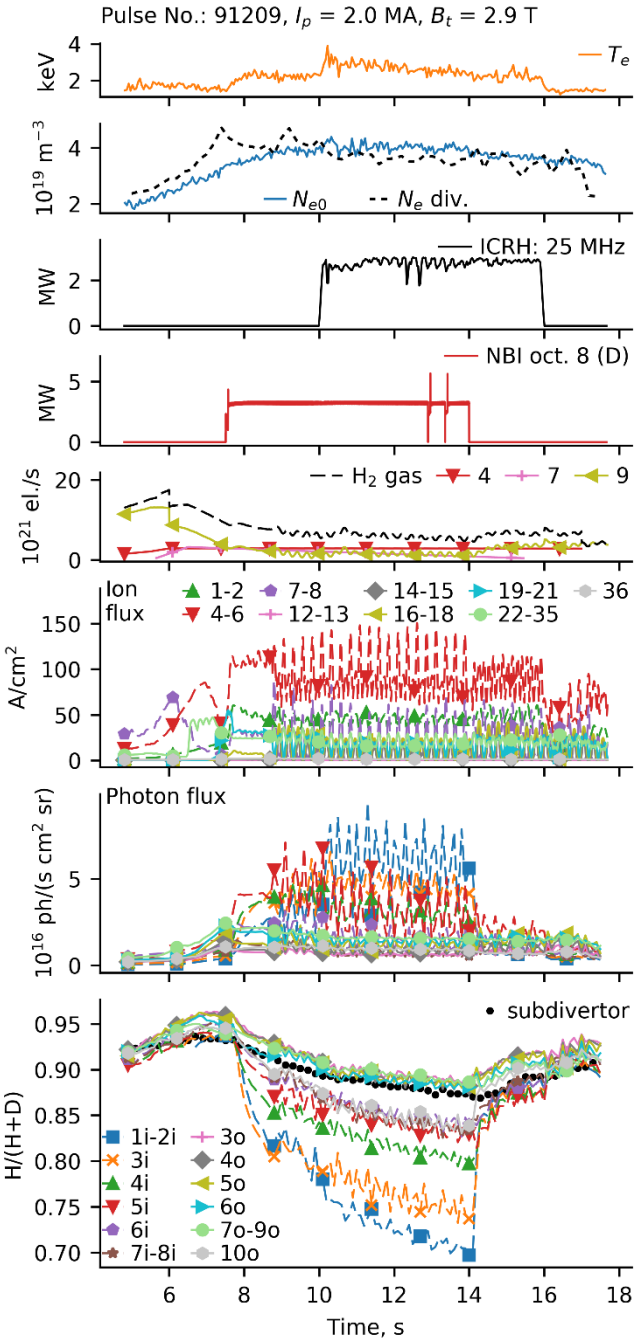

Figure 10. Time evolution of the pulse 91209 (L-mode). See the captions of figure 7. The fourth plot from the top shows the NBI power. The label indicates that deuterium is injected by the NBI module located in the 8th octant.

Finally, we show the results for the pulse in L-mode with D-NBI. Figure 11 shows the time evolution of the pulse 91211.The locations of the inner and outer strike points are the same as in the pulse 91100 shown in figure 8 but the time interval is different: 4 s < t < 9.5 s. Except the very beginning and very end of the discharge, the divertor GIMs 9 – 12 are used here for gas puffing. When the GIMs 10 and 12 are used, one can see the increase of the electron density in the divertor measured on the vertical LoS (R = 2.7 m) of the far infrared interferometer. D_2 and H_2 are introduced with the same rates via the GIMs located in the inner and outer divertor respectively. This leads to increase of deuterium concentration in the inner divertor and the hydrogen concentration in the outer divertor. Between the 4th and 10th seconds the H/(H+D) ratio on the LoSs 1i – 5i is lower than that on the LoSs 3o – 9o by about 0.2. The signal on the LoSs 5i and 6i exhibit the highest Balmer-alpha photon flux among all the LoSs that correlates with the high ion flux registered by the probes 4 – 8. The figures for some other pulses with D- and/or

H-NBI in L-mode: 91212, 91213, 91221, 91227, 91229, 91230, 91267 – 91271 can be found in the supplementary material. All of them feature very similar spatial distribution of hydrogen concentration in the divertor.

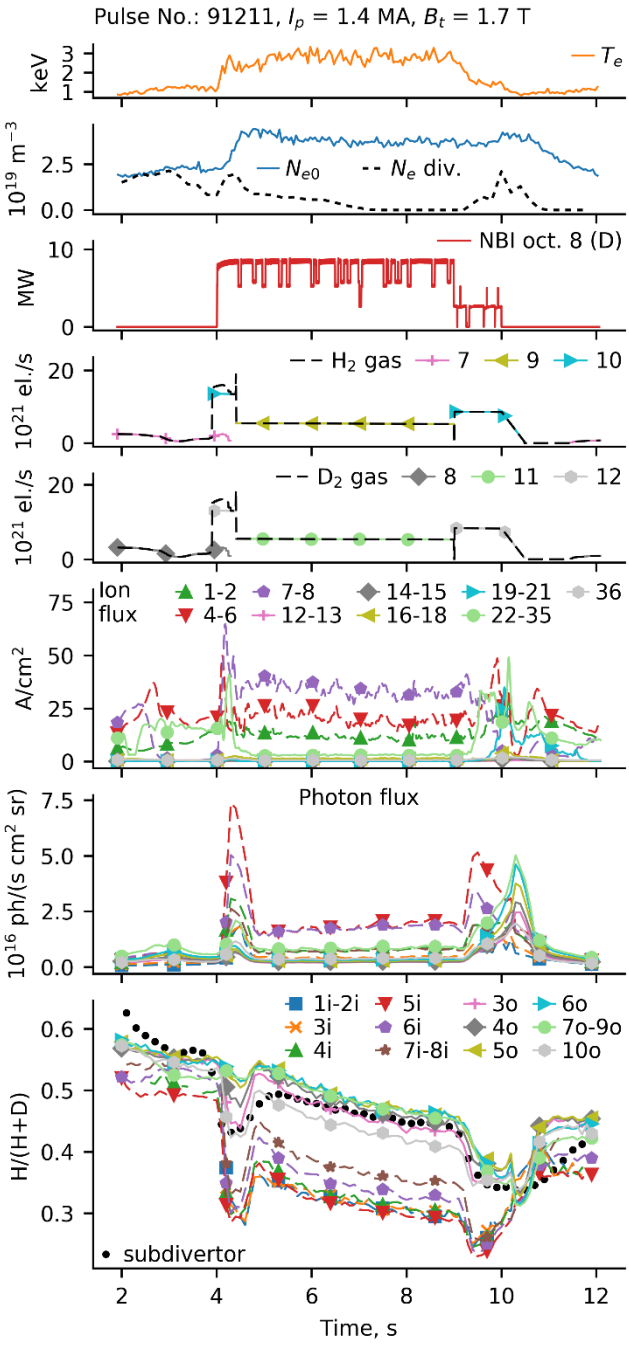

Figure 11. Time evolution of the pulse 91211 (L-mode). See the captions of figures 7 and 10.

The gases injected via the GIMs located in the inner and outer divertor are swapped in the pulses 91340 – 91344 which results in higher H/(H+D) ratio in the inner divertor starting with the pulse 91341. The figures for the pulses 91340, 91341 and 91343 can be found in the supplementary material.

In the last day of the C37 campaign after two weeks of operation in H-only plasma, the deuterium was introduced in the vessel again. Since the significant amount of hydrogen is trapped in the tiles 0 and 1, one could expect the excess of hydrogen in the inner divertor. However, the injection of D_2 via the inner divertor GIMs 11 and 12 mitigated possible effects caused by desorption of trapped hydrogen. The figures for the pulses 91742, 91745, 91747, 91749, 91751 – 91756 can be found in the supplementary.

In these pulses, the spatial distribution of hydrogen concentration in the divertor is close to that in the pulse 91211 shown in figure 11.

As for the H/(H+D) ratio in the subdivertor, this curve is always smoother than any curve for the divertor: it responds slower to the jumps in the gas injection rate. Also due to the trapped hydrogen in the Penning gauge during the previous pulse(s), in the beginning of the pulses 91017, 91100 and 91211 shown in the figures 8, 9 and 11 respectively the curve shows slightly higher hydrogen concentration than that in the divertor. The physics behind the behaviour of the subdivertor curve in the case of D-T plasma is explained in [22]. In all cases the H/(H+D) ratio measured in the subdivertor was closer to the H/(H+D) ratio in the outer divertor than to that in the inner divertor.

Here we do not show the results for the pulses with deuterium pellet injection. Such figures for the pulses 91240, 91243 – 91246, 91384 – 91387, 91389, 91392 and 91393 are available in the supplementary material. During the injection of deuterium pellets, the deuterium concentration significantly increases on all LoSs. At the same time, the difference between the H/(H+D) ratio in the inner and outer divertor is lower than 0.15 despite the simultaneous ICRH and/or NBI power are present.

The quantitative analysis of all the processes involved in the inhomogeneous distribution of hydrogen isotopes in the divertor of JET-ILW requires complex numerical simulations and is out of the scope of this paper.

Spatially-resolved measurements of the isotope ratio in the divertor are needed in the upcoming D-T experiment too. However, the correct interpretation of the HRS spectra in D-T plasma is much more difficult task than in the H-D plasma.

3. Determination of isotope ratio in D-T plasma.

The distance between the Dα and Hα line centres is 0.177 nm, for the Dα and Tα lines the respective distance is three times smaller: 0.059 nm. Due to the Doppler broadening, the Dα and Tα lines almost merge into a single line in the measured spectra. As a result, the isotope ratio becomes harder to determine. Possible line shape asymmetry not considered in the S^{theor} model spectra (1) was not a problem in the case of H-D plasma. Even if the fit of the measured spectrum was imperfect due to this asymmetry, the isotope ratio was still determined with high accuracy because the Dα and Hα lines overlap only partially (see figure 2). Here we will show that in the case of D-T plasma even weak asymmetry of the Dα line shape can be misinterpreted by the inverse problem's solver as a small contribution of the Tα line (see figure 12) and vice versa, the solver can ignore a small contribution of the Dα line if the Tα line shape is slightly asymmetric (see figure 18). The fact that this problem reduces the accuracy of determination of tritium concentration was mentioned in [23] as applied to the DTE1 experiment.

The parametric model of asymmetric line shape prompted by the ballistic model for penetration of neutral atoms into the plasma [24, 25] was developed previously [10] for interpreting the measurements in the main chamber SOL [7], where the asymmetry induced by the net inward flux of neutral atoms (due to the reflection of atoms from the wall and the combined recombination/reflection of ions) is much stronger than that in the divertor due to much lower plasma density. The same model can be applied to the measurements in the divertor as well. This model generalizes the S^{theor} model spectrum by introducing additional non-Maxwellian group of atoms. Then for the π-component of Zeeman triplet, we have the following model of Balmer-alpha line shape:

$$S^{\text{theor}}_{\text{Asymm}}(\lambda_j) = \sum_{i=\text{H,D,T}} X_i \left(\sum_{t=1}^{M} x_t \, F_{\text{Gauss}}\left(\lambda_j - \lambda_i^{\text{alpha}}, T_t\right) + x_{\text{nm}} \tilde{F}_{\text{Asymm}}\left(\lambda_j - \lambda_i^{\text{alpha}}, T_{\text{nm}}, \Lambda_{\text{nm}}\right) \right), \quad (6)$$

$$\tilde{F}_{\text{Asymm}}(\lambda) = \frac{F_{\text{Asymm}}(\lambda)}{\int F_{\text{Asymm}}(\lambda) d\lambda} \quad (7)$$

$$F_{\text{Asymm}}(\lambda_j) = F_{\text{Gauss}}\left(\lambda_j - \lambda_i^{\text{alpha}}, T_{\text{nm}}\right) \exp\left(-\Lambda_{\text{nm}} / \left|\lambda_j - \lambda_i^{\text{alpha}}\right|\right) \eta\left(\lambda_i^{\text{alpha}} - \lambda_j\right). \quad (8)$$

Here $\eta(\lambda)$ is the Heaviside function. Compared to the S^{theor} spectrum, this one has three additional sought-for parameters: T_{nm} is the effective temperature of non-Maxwellian atoms, x_{nm} is the partial contribution (statistical weight) of the non-Maxwellian atoms, Λ_{nm} is the characteristic wavelength shift for the spectral contribution of the non-Maxwellian atoms, which describes the attenuation of the inward flux. With $M = 3$ for the mixture of three isotopes, the inverse problem has 11 sought-for parameters. Note that a small fraction of hydrogen (~1 − 2%) is always present in JET. The $S^{\text{theor}}_{\text{Asymm}}$ spectrum with $M = 2$ was used in [13] for fitting the Dα spectra in the divertor of JET (see figure 10 there). When using the $S^{\text{theor}}_{\text{Asymm}}$ spectrum in the case of D-T plasma, it is very important to properly set the constraints for the sought-for parameters. All the experimental data shown below were processed with different constraints. The most stable results with $M = 3$ were achieved with the following constraints: 0.5 eV < T_1 < 5 eV, 3 eV < T_2 < 30 eV, 15 eV < T_3 < 200 eV, 15 eV < T_{nm} < 200 eV, 0.005 nm < Λ_{nm} < 0.1 nm. With $M = 2$ the constraints for T_{nm} and Λ_{nm} are the same while the constraints for T_1 and T_2 are: 0.5 eV < T_1 < 10 eV, 5 eV < T_2 < 200 eV.

To demonstrate that the solver which uses the S^{theor} spectrum can misinterpret the asymmetry of Dα line as a contribution of tritium, we processed the deuterium pulse 92324, with the freedom for the solver to search for tritium. Figure 12 shows the best fits of the spectrum on the LoS 7o at $t = 6.2$ s with the model spectra S^{theor} and $S^{\text{theor}}_{\text{Asymm}}$. In both cases the presence of tritium was allowed, but only using the S^{theor} spectrum the solver falsely found it.

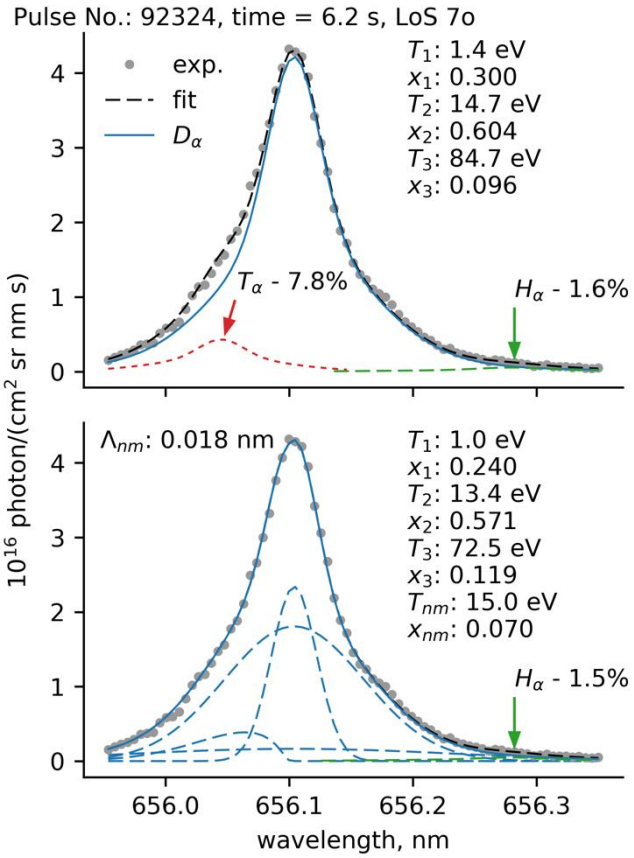

Figure 12. Best fit of the spectrum on the LoS 7o at $t = 6.2$ s of the deuterium pulse 92324 with the model spectra S^{theor} (1) (top) and $S^{\text{theor}}_{\text{Asymm}}$ (6) (bottom). The optimal parameters of the models are shown. Using the S^{theor} spectrum the solver falsely found 7.8% of tritium.

Of course, using the $S^{\text{theor}}_{\text{Asymm}}$ spectrum does not guarantee that there will be no errors. Figure 13 shows the time dependence of the tritium concentration, T/(H+D+T), found in the deuterium pulse 92324 for the lines of sight 3o – 10o with three model spectra: S^{theor}, $S^{\text{theor}}_{\text{Asymm}}$ with $M = 3$ and $S^{\text{theor}}_{\text{Asymm}}$ with $M = 2$.

The deviation of the curves from zero shows the error in each case. The most accurate result is achieved when the $S^{\mathrm{theor}}_{\mathrm{Asymm}}$ spectrum is used with $M = 3$ but even in this case the solver falsely detected up to 5% of tritium on the LoS 10o. We will show below that using the S^{theor}_{CW} spectrum (3) also results in overestimation of tritium concentration (see figures 17 and 18) but the error is smaller than that for the S^{theor} spectrum.

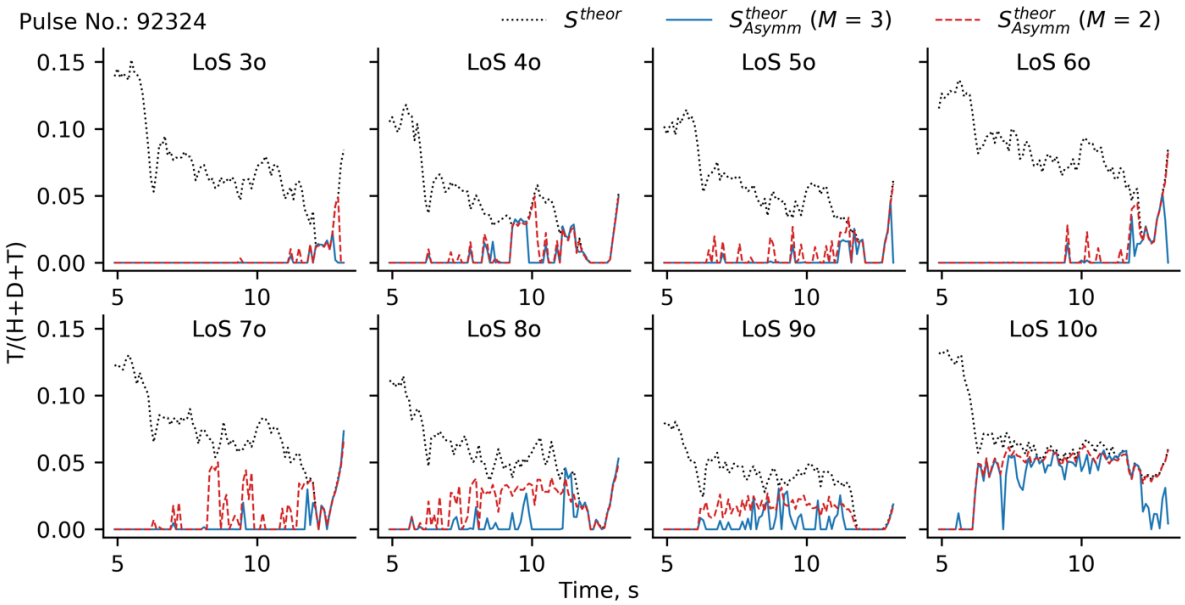

Figure 13. Time dependence of the tritium concentration, T/(H+D+T), found in the deuterium pulse 92324 for the lines of sight 3o – 10o with three model spectra: S^{theor} (1), $S^{\mathrm{theor}}_{\mathrm{Asymm}}$ with $M = 3$ and $S^{\mathrm{theor}}_{\mathrm{Asymm}}$ with $M = 2$ (6). The deviation of the curves from zero shows the error in each case.

Just as the S^{theor} spectrum tends to overestimate the tritium concentration, the $S^{\mathrm{theor}}_{\mathrm{Asymm}}$ spectrum may tend to do the opposite. The only way to test the $S^{\mathrm{theor}}_{\mathrm{Asymm}}$ model spectrum on the mixed Dα and Tα signals is to turn to the data of the DTE1 experiment carried out at JET in 1997 [26, 27, 28].

During the DTE1, the HRS in divertor had only 8 lines of sight, which layout is shown in figure 14. The resolution of the spectrometer was twice lower than now and equal to 0.0107 nm/pixel. The σ-components of Zeeman triplet were filtered out.

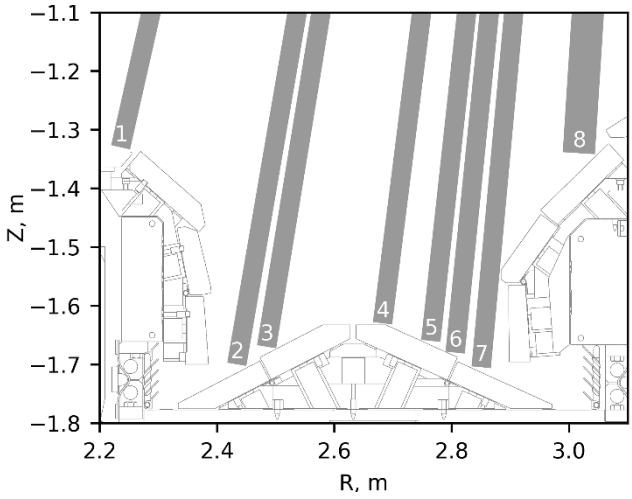

Figure 14. The layout of LoSs 1 – 8 of the divertor of JET-C during the DTE1 campaign. The bars show projections of observation cones on the poloidal plane.

The Balmer-alpha spectra on all LoSs measured at t = 15.5 s of the pulse 42752 of the DTE1 and their best fit with the $S^{\text{theor}}_{\text{Asymm}}$ model spectra are shown in figure 15. Such relation of signals and line widths on the LoSs during the flat-top as shown in figure 15 was observed in most of the pulses of the DTE1. The LoS 4 is characterized by the highest asymmetry of the line shape (x_{nm} = 0.23) and largest line shape width among all LoSs. The greater the width and the asymmetry of the line shape are, the more difficult is to separate the Dα and Tα lines. One can expect that the value of tritium concentration on the LoS 4 should be lying between the respective values on the neighbouring LoSs, however the determined values of T/(H+D+T) ratio are: 0.44, 0.41 and 0.49 on the LoSs 3, 4 and 5, respectively. It is very likely that tritium concentration on the LoS 4 is underestimated by 0.03 at least. At the same time, the $S^{\text{theor}}_{\text{Asymm}}$ spectrum works much better than the S^{theor} spectrum which for the LoSs 3, 4 and 5 gives the values of T/(H+D+T) ratio: 0.45, 0.59 and 0.53. respectively. During the DTE1 the standard software for interpreting the HRS spectra, which uses the model spectrum S^{theor}_{CW} (3), was processing the data from the LoS 7 only. For the data of figure 15, the T/(H+D+T) ratio obtained with the S^{theor}_{CW} spectrum is 0.51 versus 0.48 obtained with the $S^{\text{theor}}_{\text{Asymm}}$ spectrum.

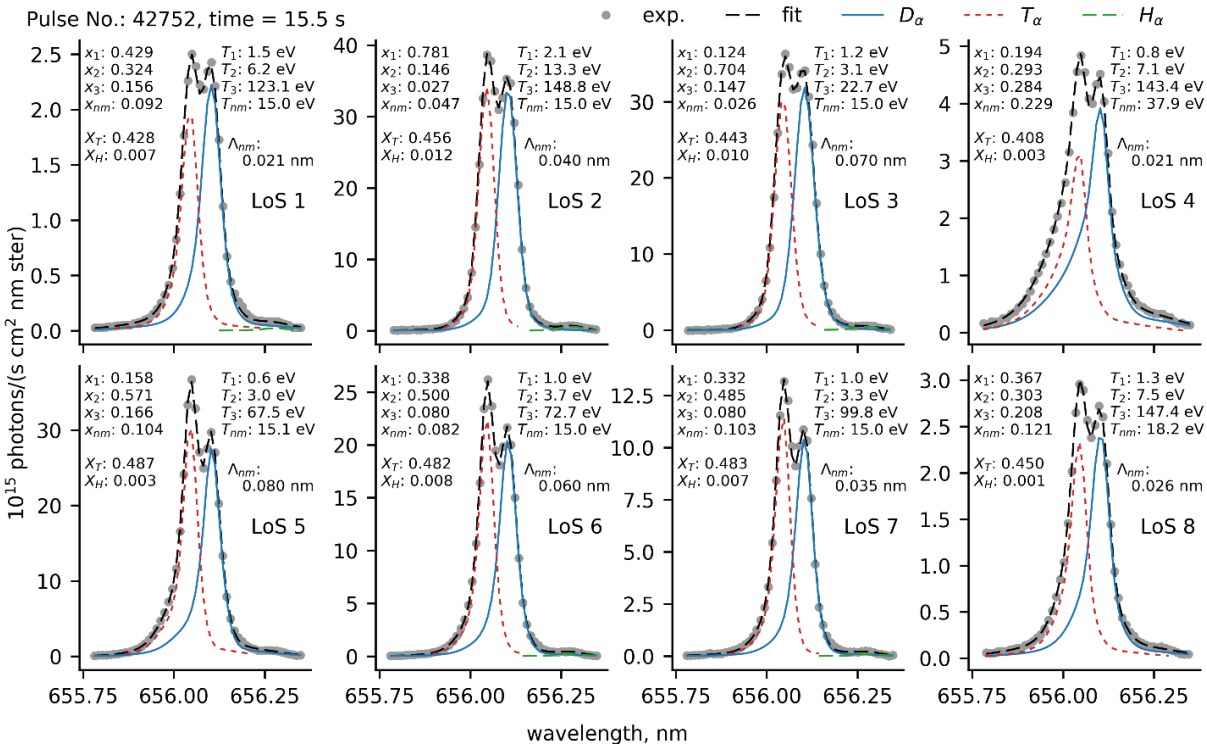

Figure 15. Best fit of the experimental spectra on 8 LoSs with the theoretical spectra $S^{\text{theor}}_{\text{Asymm}}$ (6) at time t = 15.5 s of the pulse 42752 of the DTE1 campaign. The optimal parameters of the $S^{\text{theor}}_{\text{Asymm}}$ are shown.

During the DTE1 campaign on JET-C the divergence between the isotope ratio measured on different LoSs was much smaller than that shown in section 2 for the C37 campaign on JET-ILW. Processing of all pulses of the DTE1 with significant amount of tritium showed that the difference in tritium concentration on different LoSs rarely exceeded 0.1. Figure 16 shows the time evolution of the pulse 42752 where the GIM 15 was used for T_2 puffing. Note that the T/(H+D+T) ratio for the LoS 4 is shown with dashed curve because of the low accuracy for this LoS. Although the tritium concentration increases threefold during the discharge, the maximum difference in tritium concentration on different LoSs does not exceed 0.08. In the pulses of the DTE1 there was no simple correlation between the Balmer-alpha photon flux and the isotope ratio. In figure 16 one can see that the increase of the photon flux on the LoS 2 is correlated with the increase of the T/(H+D+T) ratio on the same LoS. Such correlation is observed for the LoS 2 in many other pulses of the DTE1 but not for other LoSs.

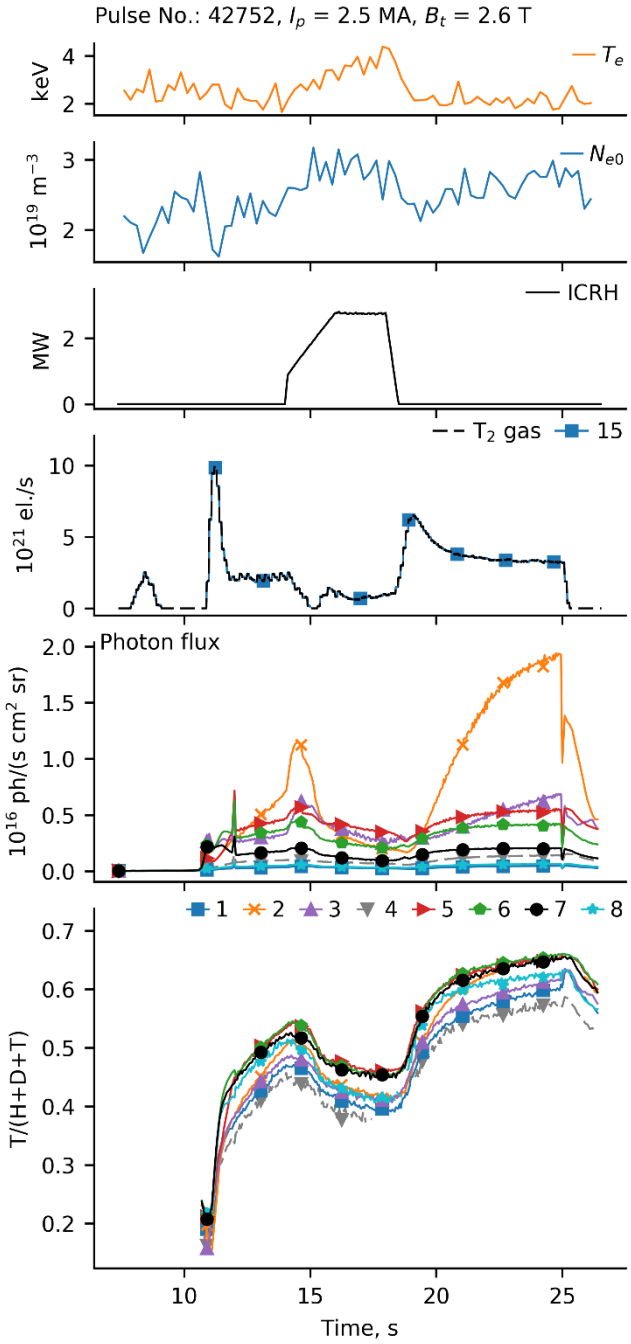

Figure 16 Time evolution of the pulse 42752. See the caption of figure 7.

To estimate the accuracy of determination of isotope ratio with the $S^{\text{theor}}_{\text{Asymm}}$ spectrum, it is necessary to compare the results for the divertor and subdivertor. Unfortunately, for many pulses of the DTE1, the Balmer-alpha signals measured in the Penning discharge were too weak. The number of photoelectrons collected by a single spectral channel (pixel) in a single measurement rarely exceeded 1000. A high statistical noise reduces the accuracy of the result, yet in some pulses the signals were strong enough (> 400 photoelectrons at spectrum's maximum) to perform a benchmark. Figure 17 shows the comparison of the T/(H+D+T) ratio measured on the divertor LoS 7 and in the Penning gauge in the subdivertor in the pulses 41677, 42638, 43009 and 43057. The results for the LoS 7 are given for three model spectra: S^{theor}, S^{theor}_{CW} и $S^{\text{theor}}_{\text{Asymm}}$. The detailed figures similar to figure 16 for these 4 pulses can be found in the supplementary material. For the S^{theor}_{CW} spectrum, the T/(H+D+T) ratio is determined using the cold

fraction of atoms only. The difference between the values of $X_{c,T}$ and $X_{cw,T}$ (4) is about 0.01 for the pulses of the DTE1.

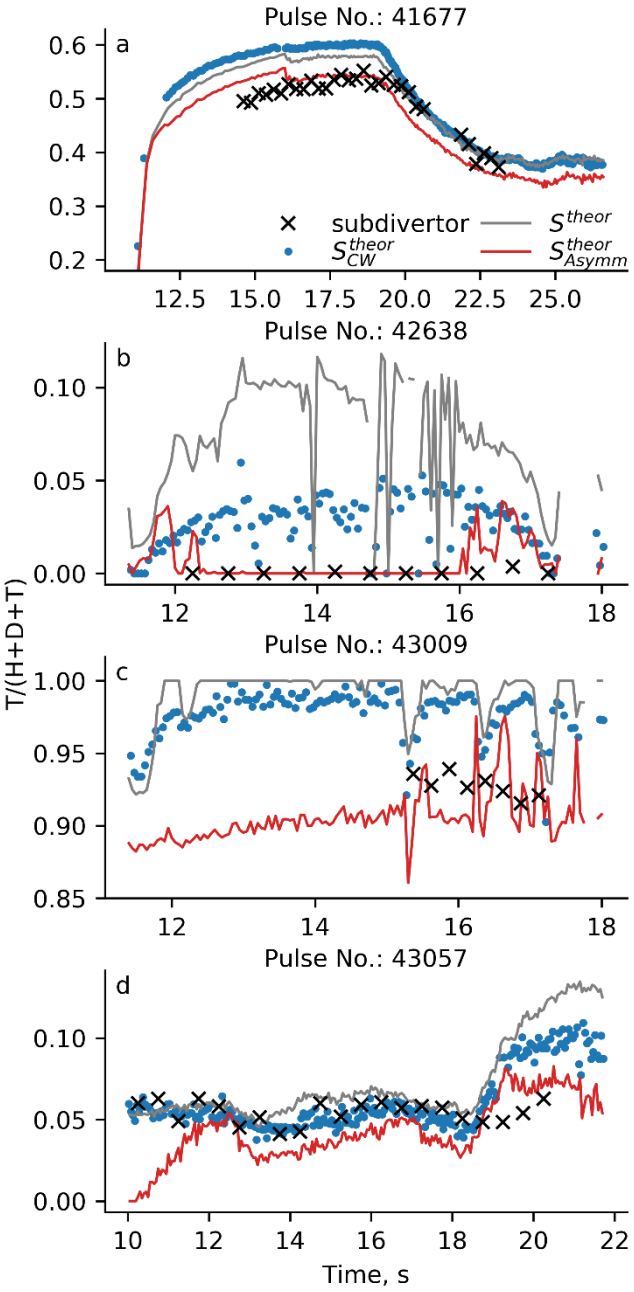

Figure 17. The comparison of the T/(H+D+T) ratio measured on the divertor LoS 7 and in the Penning gauge in the subdivertor in the pulses 41677 (a), 42638 (b), 43009 (c) and 43057 (d). The results for the LoS 7 are given for three model spectra: S^{theor} (1), S^{theor}_{CW} (3) и S^{theor}_{Asymm} (6).

Now we consider each of 4 pulses in details. In the pulse 41677 (figure 17 a) the T_2 is injected via GIM 15 with the rate slowly decreasing after t = 12 s. This injection stops at t = 19 s and starts again at t = 23 s at low rate. The ICRH starts at t = 19 s, reaches its maximum of 7 MW at t = 22 s and stops at t = 25 s. Two short (~0.2 s) D-NBI pulses take place at t = 16 s and t = 25 s, first of which is correlated with small but noticeable drop of the T/(H+D+T) ratio in the curves for the S^{theor} and S^{theor}_{Asymm} model spectra. Unlike most of the pulses of the DTE1 here the tritium concentration obtained with the S^{theor}_{CW} spectrum is even higher than that obtained with the S^{theor} spectrum. As expected, the curve for subdivertor is

smoother than three other curves. When the tritium concentration reaches a plateau (16 s < t < 19 s), the subdivertor curve shows the same T/(H+D+T) ratio as the $S^{\text{theor}}_{\text{Asymm}}$ curve does.

The pulse 42638 (figure 17 b) allows to compare the results in the case when the tritium concentration is known to be smaller than 0.01. The pulse 41770 was the last one before the pulse 42638 when the tritium was injected into the plasma. Then for 3 months tritium was removed from the vessel with the help of ICRH which heats up the first wall. Both, the residual gas analyser and the neutron rate detector, show that by the time of the pulse 42638 the tritium concentration in the vessel was lower than 0.003 (see figure 5 in [29]). Of course, the HRS cannot detect such small fractions of tritium, that's why the subdivertor curve shows zero. Figure 17 shows that the S^{theor} spectrum gives the highest error for T/(H+D+T) ratio, 0.1. The error of the S^{theor}_{CW} spectrum is about 0.03 – 0.05. The $S^{\text{theor}}_{\text{Asymm}}$ spectrum gives the most accurate result, yet at the beginning and at the end of discharge it also gives an error about 0.03.

Starting from the pulse 42640, tritium was injected into the plasma again. In the pulse 43009 (figure 17 c), the tritium concentration exceeds 0.9. The intense injection of T_2 during the time interval: 12 s < t < 17 s is accompanied by 4 MW ICRH, which increases the release of deuterium trapped in the wall. When the S^{theor} is used, the solver fails to detect deuterium and gives unrealistic result of 100% tritium concentration. The result of the S^{theor}_{CW} spectrum (98% – 99% tritium concentration) looks more realistic, yet it appears that the solver also fails to detect deuterium and the remaining 1% – 2% is a contribution of hydrogen. Figure 18 shows the best fit of the the experimental spectrum on LoS 7 with the theoretical spectra $S^{\text{theor}}_{\text{Asymm}}$ and $S^{\text{theor}}_{\text{cw}}$ at time t = 13.5 s of the pulse 43009. One can see that unlike the $S^{\text{theor}}_{\text{Asymm}}$ spectrum, the $S^{\text{theor}}_{\text{cw}}$ does not reproduce well the experimental data in the range between 656.08 nm and 656.18 nm smoothing out the weak but noticeable Dα peak. The same happens in other time moments of this pulse, as well as in some other pulses. The values of the T/(H+D+T) ratio in subdivertor are in good agreement with those obtained with the $S^{\text{theor}}_{\text{Asymm}}$ spectrum. However, the T/(H+D+T) ratio in divertor and in subdivertor do not have to match in this case because some amount of deuterium could be accumulated in the vacuum tube during the previous pulses. So, the correct values of the tritium concentration may be slightly higher than those showed by the $S^{\text{theor}}_{\text{Asymm}}$ curve.

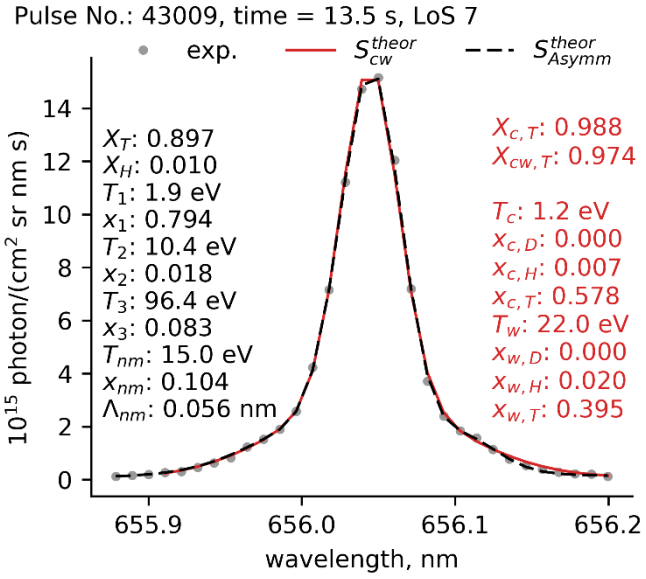

Figure 18. Best fit of the experimental spectrum on LoS 7 with the theoretical spectra $S^{\text{theor}}_{\text{Asymm}}$ (6) and $S^{\text{theor}}_{\text{cw}}$ (3) at time t = 13.5 s of the pulse 43009. The optimal parameters of the $S^{\text{theor}}_{\text{Asymm}}$ and $S^{\text{theor}}_{\text{cw}}$ are shown in the left and right columns respectively.

After the pulse 43023, tritium is no longer injected into the plasma, and by the time of the pulse 43057 (figure 17 d) its concentration in the vessel goes down to ~0.05. For this pulse, the results of all three

model spectra coincide quite well not only with each other but also with the results in the subdivertor. However, before t = 12 s the $S_{\mathrm{Asymm}}^{\mathrm{theor}}$ spectrum underestimates the T/(H+D+T) ratio, probably confusing weak Tα peak with the asymmetry of Dα line. By processing this pulse, we can estimate the lower limit of tritium concentration which can be reliably determined using the $S_{\mathrm{Asymm}}^{\mathrm{theor}}$ spectrum as 0.04 – 0.05.

Now we compare the time-average tritium concentrations, obtained with different model spectra. Figure 19 shows the time-average T/(H+D+T) ratio for 254 pulses of the DTE1 obtained in 4 different ways, namely: (i) using the $S_{\mathrm{Asymm}}^{\mathrm{theor}}$ spectrum and averaging over the LoSs (excluding the LoS 4), (ii) using the S^{theor} spectrum and averaging over the LoSs (excluding the LoS 4), (iii) using the $S_{\mathrm{Asymm}}^{\mathrm{theor}}$ spectrum for the LoS 7 only, (iv) using the S_{CW}^{theor} spectrum for the LoS 7 only. The time-average T/(H+D+T) ratio in subdivertor was calculated using only those measurements for which at least one spectral channel (pixel) collected more than 400 photoelectrons and only if the number of such measurements were greater than 5 Therefore, in figure 19 the values of the time-average T/(H+D+T) ratio in the subdivertor are given only for 132 pulses out of 254. One can compare figure 19 with figure 5 in [29] which shows the tritium concentration for all pulses of the DTE1.

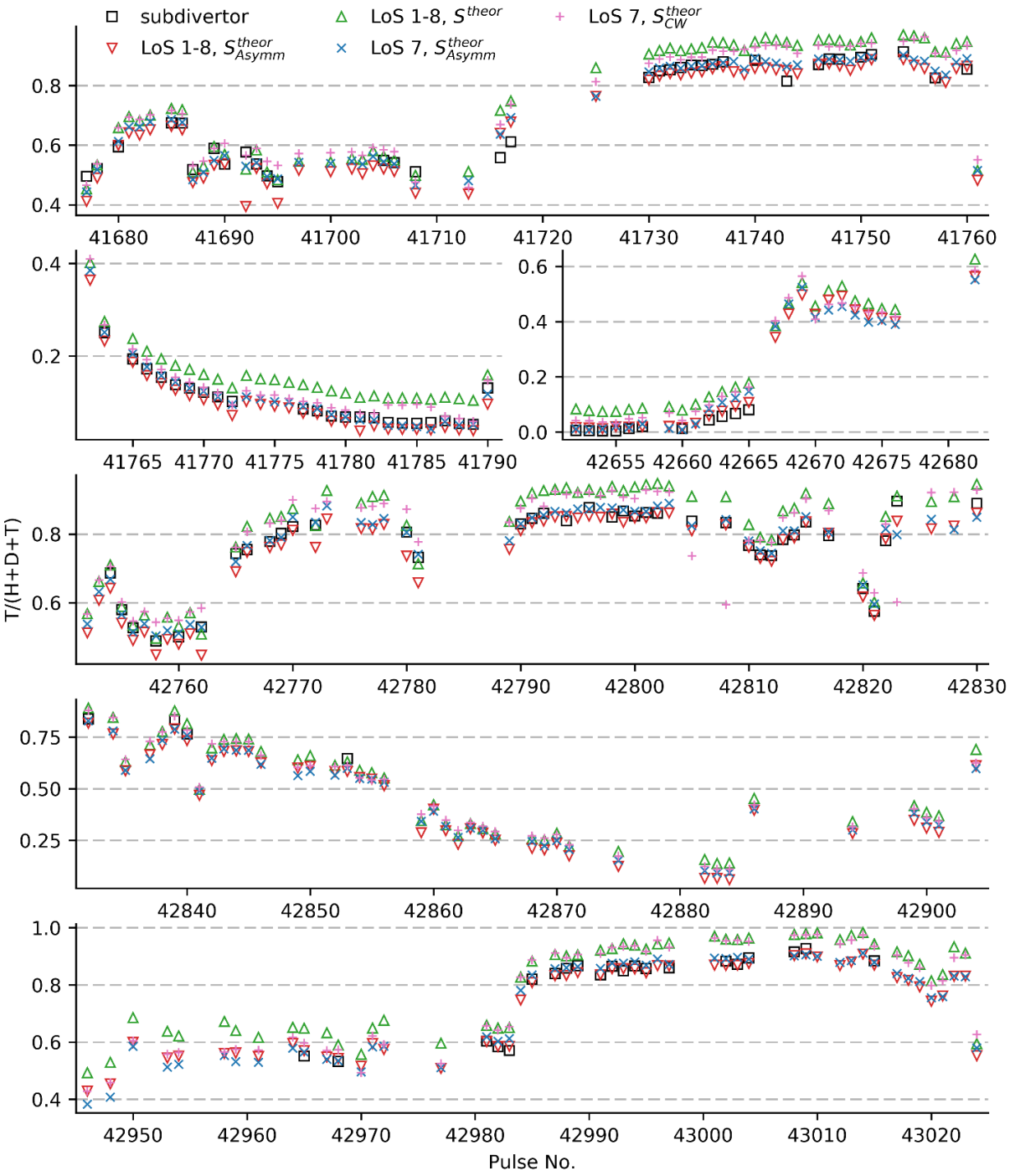

Figure 19. Time-average T/(H+D+T) ratio in divertor for 254 pulses of the DTE1 obtained in different ways. In the legend: LoS 1-8 means averaging over the LoSs excluding the LoS 4. S^{theor}, S^{theor}_{CW} and $S^{\text{theor}}_{\text{Asymm}}$ denote the model spectrum used.

One can see form figure 19 that, first, the time- and LoS-average tritium concentration obtained with the S^{theor} spectrum is always higher than that obtained with the $S^{\text{theor}}_{\text{Asymm}}$ spectrum, and the difference between these two sometimes exceeds 0.1. Second, the tritium concentration on the LoS 7 obtained with the S^{theor}_{CW} spectrum is usually higher than that obtained with the $S^{\text{theor}}_{\text{Asymm}}$ spectrum, and the difference between these two increases with the increase of tritium concentration. Third, the tritium concentration on the LoS 7 obtained with the $S^{\text{theor}}_{\text{Asymm}}$ spectrum is closest among all to that in subdivertor. The latest can be shown by calculating the average absolute deviation of each set of results in the divertor from the tritium concentration in the subdivertor:

$$\Delta X_T^{\mathrm{sub}} = \frac{1}{N^{\mathrm{sub}}} \sum_{p=1}^{N^{\mathrm{sub}}} \left| \left[X_T^{\mathrm{div}}\right]_p - \left[X_T^{\mathrm{sub}}\right]_p \right|. \quad (8)$$

Here p is the pulse index, $N^{\mathrm{sub}} = 132$ is the total number of pulses, the brackets […] denote averaging over time. For each set of results in figure 19 for the $\Delta X_T^{\mathrm{sub}}$ we have:

LoS 1-8, S^{theor}:	0.057
LoS 7, S_{CW}^{theor}:	0.048
LoS 1-8, $S_{\mathrm{Asymm}}^{\mathrm{theor}}$:	0.023
LoS 7, $S_{\mathrm{Asymm}}^{\mathrm{theor}}$:	0.016

However, the time-average tritium concentration in divertor and subdivertor may differ for physical reasons, so some uncertainty still remains.

The $S_{\mathrm{Asymm}}^{\mathrm{theor}}$ spectrum fits the experimental data better than the S^{theor} and S_{CW}^{theor} spectra do and allows for more accurate determination of tritium concentration. Yet even with the $S_{\mathrm{Asymm}}^{\mathrm{theor}}$ spectrum the error of obtained tritium concentration is about 0.03 – 0.05 for the measurements with negligible statistical noise while for hydrogen concentration its only 0.01 – 0.02.

4. Conclusions

Processing the data from the Hα high resolution spectroscopy (HRS) on JET with the help of the updated interpretation model gave the following results.

1. Spatially-resolved measurements of the isotope ratio in the divertor of JET-ILW revealed that in many pulses of recent C37 campaign in the H-D plasma the hydrogen concentration, H/(H+D), in the inner divertor was lower than that in the outer divertor by 0.15 – 0.35, depending on plasma configuration and heating parameters.

2. The typical scheme of gas puffing used in many pulses of the C37 campaign, namely the injection of D_2 via the gas introduction modules (GIMs) 11 and 12 located in the inner divertor and H_2 via the GIMs 9 and 10 located in the outer divertor, creates spatial inhomogeneity of the isotope ratio in the divertor plasma during the gas puffing. It is very likely that the divertor tiles 0, 1 and 3 absorb some of the deuterium injected via the GIMs 11 and 12 and release it during the subsequent pulses in the cases where the heat loads on the divertor tiles are high enough, e.g. due to the use of ICRH. This results in higher deuterium concentration in the inner divertor even in those pulses where the divertor GIMs are not used. The quantitative analysis of this process however requires complex numerical simulations.

3. For interpretation of spatially-resolved HRS measurements in divertor in the upcoming D-T experiment we suggest using the model of asymmetric line shape [10] because it improves the accuracy of determination of the isotope ratio.

4. The test of the model [10] against the data of the first D-T experiment on JET-C, the DTE1, showed that this model has the following benefits compared to the model used during the DTE1: (i) the model fits the experimental spectra better, (ii) it allows to detect smaller deuterium concentration in tritium-dominated plasma, (iii) in the most measurements, it does not falsely detect tritium in deuterium-only pulses, (iv) it gives better agreement between the time-average tritium concentration measured in outer divertor and in the Penning gauge in subdivertor. Yet even with the model of asymmetric line shape the error of obtained tritium concentration is about 0.03 – 0.05 while for hydrogen concentration it is only 0.01 – 0.02.

Acknowledgments. This work was supported by the RF State Corporation Rosatom and Euratom, and carried out within the framework of cooperation between the EUROfusion Consortium and Rosatom. This work has been carried out within the framework of the EUROfusion Consortium and has received funding from the Euratom research and training programme 2014–2018 under grant agreement no. 633053. The authors thank A.G. Alekseev, E.N. Andreenko, A.V. Gorshkov, M.B. Kadomtsev, V. Kotov, M.G. Levashova, S.W. Lisgo, V.S. Lisitsa, V.A. Shurygin, E. Veshchev, D.K. Vukolov and

K.Yu. Vukolov for their collaboration in the studies on the ITER main chamber H-alpha (and visible light) spectroscopy diagnostics, A.A. Pshenov and A.S. Kukushkin for helpful advices, A. Shaw for helpful discussions on spectroscopy at JET and Ph. Jacquet for providing figure 5.

The views and opinions expressed herein do not necessarily reflect those of the European Commission.

References

[1] Nunes I. *et al* Proc. 26th Int. Conf. on Fusion Energy (Kyoto, 2016) PDP-2 (https://infoscience.epfl.ch/record/226118/files/Nunes_Weisen_IAEA_postdeadline_V4.pdf)
[2] King D.B. *et al* 2017 *Proc. 44th EPS Conference on Plasma Physics (Belfast, United Kingdom, 26-30 June 2017)* O3.112 (http://ocs.ciemat.es/EPS2017PAP/pdf/O3.112.pdf)
[3] Maggi C.F. *et al* 2018 *Plasma Phys. Control. Fusion* **60** 014045 (https://doi.org/10.1088/1361-6587/aa9901)
[4] Huber A. *et al* 2018 *Nucl. Fusion* **57** 086007 (https://doi.org/10.1088/1741-4326/aa663a)
[5] Ongena J. *et al* 2017 *EPJ Web of Conferences* **157** 02006 (https://doi.org/10.1051/epjconf/201715702006)
[6] Van Eester D. *et al* 2017 *EPJ Web of Conferences* **157**, 03061 (https://doi.org/10.1051/epjconf/201715703061)
[7] Neverov V.S., Kukushkin A.B., Stamp M.F., Alexeev A.G., Von Hellermann M. and JET Contributors 2017 *Nucl. Fusion* **57** 016031 (https://doi.org/10.1088/0029-5515/57/1/016031)
[8] Kukushkin A.B. *et al* 2014 Proc. 25th IAEA Fusion Energy Conf. (St. Petersburg, Russia, 13–18 October 2014) EX/P5-20 (Preprint EFDA-JET-CP(14)06/33) (www.euro-fusionscipub.org/wp-content/uploads/2015/04/EFDC140633.pdf)
[9] Kajita S. *et al* 2013 *Plasma Phys. Contr. Fusion* **55** (8) 085020 (https://dx.doi.org/10.1088/0741-3335/55/8/085020)
[10] Kukushkin A.B., Neverov V.S., Kadomtsev M.B., Kotov V., Kukushkin A.S., Levashova M.G., Lisgo S.W., Lisitsa V.S., Shurygin V.A. and Alekseev A.G. 2014 *J. Phys.: Conf. Ser.* **548** 012012 (https://dx.doi.org/10.1088/1742-6596/548/1/012012)
[11] Neverov V.S., Kukushkin A.B., Lisgo S.W., Kukushkin A.S. and Alekseev A.G. 2015 *Plasma Phys. Rep.* **41** 103–11 (https://doi.org/10.1134/S1063780X15020075)
[12] Kukushkin A.B., Neverov V.S., Alekseev A.G., Lisgo S.W. and Kukushkin A.S. 2016 *Fusion Sci. Tech.***69** 628–42 (https://dx.doi.org/10.13182/FST15-186)
[13] Lomanowski B.A., Meigs A.G., Sharples R.M., Stamp M., Guillemaut C. and JET Contributors 2015 *Nucl. Fusion* **55** 123028 (https://dx.doi.org/10.1088/0029-5515/55/12/123028)
[14] Brezinsek S. *et al* 2016 *Phys. Scr.* **T167** 014076 (http://dx.doi.org/10.1088/0031-8949/T167/1/014076)
[15] Wiesen S. *et al* 2017 *Nucl. Fusion* **57** 066024 (https://doi.org/10.1088/1741-4326/aa69dd)
[16] Heinola K. *et al* 2015 *J. Nucl. Mater.***463** 961–965 (http://dx.doi.org/10.1016/j.jnucmat.2014.12.098)
[17] Lahtinen A.*et al* 2017 *Nucl. Mater. Energy***12** 655–661 (http://dx.doi.org/10.1016/j.nme.2017.04.007)
[18] Oya Y. *et al* 2018 *Fusion Eng. Des.* **132** 24–28 (https://doi.org/10.1016/j.fusengdes.2018.04.124)
[19] Hillis D.L., Klepper C.C., Von Hellermann M., Ehrenberg J., Finken K.H. and Mank G. 1997 *Fusion Eng. Des.* **34–35** 341–51 (https://doi.org/10.1016/S0920-3796(96)00653-9)
[20] Kazakov Ye.O., Van Eester D., Dumont R. and Ongena J. 2015 Nucl. Fusion **55** 032001 (https://dx.doi.org/10.1088/0029-5515/55/3/032001)
[21] Kazakov Ye.O. *et al* 2017 *Nature Physics* **13** 973–978 (https://dx.doi.org/doi:10.1038/nphys4167)
[22] Hillis D.L. *et al* 1999 *Phys. of Plasmas* **6** 1985–94 (http://dx.doi.org/10.1063/1.873454)
[23] Jarvis O.N., Balet B., Ehrenberg J.K., Guenther K., Howman A.C., Von Hellermann M.G., Morgan P.D., Stamp M. and Zastrow K-D. 1998 *Proc. 25th EPS Conf. on Contr. Fusion and Plasma Physics (Praha, Czech Republic, 29 June - 3 July 1998)* ECA **22C** 389–391 (http://epsppd.epfl.ch/Praha/98icpp/b185pr.pdf)

[24] Kadomtsev M.B., Kotov V., Lisitsa V.S. and Shurygin V.A. 2012 *Proc. 39th EPS Conf. 16th Int. Congress on Plasma Physics (Stockholm, Sweden, 2–6 July 2012)* P4.093 (http://ocs.ciemat.es/epsicpp2012pap/pdf/P4.093.pdf)
[25] Lisitsa V.S., Kadomtsev M.B., Kotov V., Neverov V.S. and Shurygin V.A. 2014 *Atoms* **2** 195–206 (http://dx.doi.org/10.3390/atoms2020195)
[26] Jacquinot J. and JET Team 1998 *Nucl. Fusion* **38** 1263 (https://doi.org/10.1088/0029-5515/38/9/301)
[27] Keilhacker M. *et al* 1999 *Nucl. Fusion* **39** 209 (https://doi.org/10.1088/0029-5515/39/2/306)
[28] JET Team (prepared by Watkins M.L.) 1999 *Nucl. Fusion* **39** 1227 (https://doi.org/10.1088/0029-5515/39/9Y/302)
[29] Andrew P. *et al* 1999 *J. Nucl. Mater.* **266–269** 153–159 (https://doi.org/10.1016/S0022-3115(98)00662-X)